Cellular/Molecular

The SphK1/S1P Axis Regulates Synaptic Vesicle Endocytosis via TRPC5 Channels

Zhong-Jiao Jiang and Liang-Wei Gong
Department of Biological Sciences, University of Illinois Chicago, Chicago, Illinois 60607

Sphingosine-1-phosphate (S1P), a bioactive sphingolipid concentrated in the brain, is essential for normal brain functions, such as learning and memory and feeding behaviors. Sphingosine kinase 1 (SphK1), the primary kinase responsible for S1P production in the brain, is abundant within presynaptic terminals, indicating a potential role of the SphK1/S1P axis in presynaptic physiology. Altered S1P levels have been highlighted in many neurologic diseases with endocytic malfunctions. However, it remains unknown whether the SphK1/S1P axis may regulate synaptic vesicle endocytosis in neurons. The present study evaluates potential functions of the SphK1/S1P axis in synaptic vesicle endocytosis by determining effects of a dominant negative catalytically inactive SphK1. Our data for the first time identify a critical role of the SphK1/S1P axis in endocytosis in both neuroendocrine chromaffin cells and neurons from mice of both sexes. Furthermore, our Ca^{2+} imaging data indicate that the SphK1/S1P axis may be important for presynaptic Ca^{2+} increases during prolonged stimulations by regulating the Ca^{2+} permeable TRPC5 channels, which per se regulate synaptic vesicle endocytosis. Collectively, our data point out a critical role of the regulation of TRPC5 by the SphK1/S1P axis in synaptic vesicle endocytosis.

Key words: **calcium; cell-attached capacitance recordings; live-cell imaging; Sphingosine-1-phosphate; synaptic vesicle endocytosis; TRPC5**

Significance Statement

Sphingosine kinase 1 (SphK1), the primary kinase responsible for brain sphingosine-1-phosphate (S1P) production, is abundant within presynaptic terminals. Altered SphK1/S1P metabolisms has been highlighted in many neurologic disorders with defective synaptic vesicle endocytosis. However, whether the SphK1/S1P axis may regulate synaptic vesicle endocytosis is unknown. Here, we identify that the SphK1/S1P axis regulates the kinetics of synaptic vesicle endocytosis in neurons, in addition to controlling fission-pore duration during single vesicle endocytosis in neuroendocrine chromaffin cells. The regulation of the SphK1/S1P axis in synaptic vesicle endocytosis is specific since it has a distinguished signaling pathway, which involves regulation of Ca^{2+} influx via TRPC5 channels. This discovery may provide novel mechanistic implications for the SphK1/S1P axis in brain functions under physiological and pathologic conditions.

Introduction

Synaptic transmission, mediated by exocytosis of synaptic vesicles, is sustained by subsequent endocytosis, an essential process to recapture and reuse membranes that have fused with the plasma membrane from exocytosis (Saheki and De Camilli, 2012; Rizzoli, 2014; Soykan et al., 2016). Synaptic vesicle endocytosis is thus indispensable for normal brain functions (Saheki and De Camilli, 2012; Rizzoli, 2014; Soykan et al., 2016), and deficiency in endocytic machinery has been highlighted in many neurologic disorders including multiple sclerosis, Huntington's disease, Parkinson's disease, and Alzheimer's disease (Cataldo et al., 2000; Schreij et al., 2016; Alsaqati et al., 2018; Kyung et al., 2018; Helbig et al., 2019; McAdam et al., 2020; Pensalfini et al., 2020; Barron et al., 2021; Kesharwani et al., 2021). Nevertheless, the precise molecular mechanisms for synaptic vesicle endocytosis are still far from being fully understood (Chanaday et al., 2019; Rennick et al., 2021).

Sphingosine-1-phosphate (S1P), a bioactive sphingolipid concentrated in the brain (Edsall and Spiegel, 1999; Karunakaran and van Echten-Deckert, 2017), is essential for normal brain functions. For example, S1P in hippocampus is critical for spatial learning as assessed by water maze test (Kanno et al., 2010) or T-maze test (Weth-Malsch et al., 2016), while S1P in hypothalamus regulates energy homeostasis by controlling feeding behaviors (Silva et al., 2014). On the other hand, altered S1P metabolism has been linked to many neurologic diseases (Ghasemi et al., 2016; Karunakaran and van Echten-Deckert, 2017; Di Pardo and

Received Aug. 3, 2022; revised Apr. 13, 2023; accepted Apr. 17, 2023.

Author contributions: Z.-J.J. and L.-W.G. designed research; Z.-J.J. and L.-W.G. performed research; Z.-J.J. and L.-W.G. analyzed data; Z.-J.J. and L.-W.G. wrote the first draft of the paper; Z.-J.J. and L.-W.G. edited the paper; Z.-J.J. and L.-W.G. wrote the paper.

This work was supported by National Institutes of Health Grant R01NS110533 (to L.-W.G.). We thank Dr. L. Lagnado for sypHy and Dr. T. A. Ryan for SynGCaMP6f.

The authors declare no competing financial interests.

Correspondence should be addressed to Liang-Wei Gong at lwgong@uic.edu.

https://doi.org/10.1523/JNEUROSCI.1494-22.2023

Maglione, 2018). In addition, fingolimod (FTY720), a S1P analog approved by Food and Drug Administration to treat multiple sclerosis (Chiba and Adachi, 2012; Ali et al., 2013), may slow down pathologic changes in the brain tissue from animal models for Alzheimer's disease (Karunakaran and van Echten-Deckert, 2017; Yin et al., 2021). These important functions of S1P within the brain under physiological and pathologic conditions reflect a role of S1P in synaptic transmission. Indeed, it has been reported that S1P modulates synaptic strength and plasticity (Kanno et al., 2010; Kempf et al., 2014; Weth-Malsch et al., 2016).

Sphingosine kinase 1 (SphK1) is the primary kinase responsible for S1P production in the brain (Fukuda et al., 2003; Bryan et al., 2008). The presynaptic SphK1 abundance (Kajimoto et al., 2007; Chan et al., 2012) indicates an involvement of the SphK1/S1P axis in synaptic transmission via presynaptic mechanisms. In line with this idea, the SphK1/S1P axis has been reported to be critical for synaptic vesicle exocytosis in neurons from both *Caenorhabditis elegans* and mice (Kajimoto et al., 2007; Chan et al., 2012). In non-neuronal cells, SphK1 has been found to be enriched on physiologically occurring early endocytic intermediates and a disruption of the SphK1/S1P axis induces significant endocytic defects (Shen et al., 2014; Young et al., 2016; Lima et al., 2017). In mouse and human brains, defects of synaptic vesicle endocytosis and altered S1P levels have been concurrently identified as pathologic features for neurodegenerative diseases including Alzheimer's disease and Huntington disease (Couttas et al., 2014; Pirhaji et al., 2016; Schreij et al., 2016; Lee et al., 2018; Di Pardo et al., 2019; McAdam et al., 2020; Pensalfini et al., 2020). However, it remains unknown whether the SphK1/S1P axis may regulate synaptic vesicle endocytosis in neurons.

In the present study, we evaluate potential functions of the SphK1/S1P axis in synaptic vesicle endocytosis by determining effects of a dominant negative catalytically inactive SphK1 ($SphK1^{DN}$) in neurons and chromaffin cells (Pitson et al., 2000; Bonhoure et al., 2006; Gomez-Brouchet et al., 2007; Z.J. Jiang et al., 2019b). Based on data from synaptophysin-pHluorin (sypHy) based live-cell imaging in neurons and cell-attached capacitance recordings in chromaffin cells, we for the first time identify a critical role of the SphK1/S1P axis in neuronal endocytosis. Furthermore, our Ca^{2+} imaging indicates that the SphK1/S1P axis may be important for presynaptic Ca^{2+} increases during prolonged stimulations via Ca^{2+} permeable TRPC5 channels, which per se regulate synaptic vesicle endocytosis. Altogether, our data point out an importance of the SphK1/S1P axis in synaptic vesicle endocytosis via TRPC5 channels in neurons.

Materials and Methods

Cultures of neurons, chromaffin cells, and HEK 293 cells

In this study, newborn pups of either sexes (postnatal day 0) from C577BL/6J (RRID: IMSR JAX:000664) mouse mating cages were used and cared in accordance with the guidelines of the National Institutes of Health, as approved by the Animal Care and Use Committee of the University of Illinois at Chicago (approval number of 19-189). Neuronal culture from cortex was prepared as describe previously (Vevea and Chapman, 2020; Z.J. Jiang et al., 2021). Briefly, cortical neurons were isolated and gently dissociated with papain (Worthington; LS003127) and mechanical disruption before plated on glass coverslips (Assistant; 41001118) coated with poly-D-lysine (Sigma; P0899). Neurons were maintained in Neurobasal-A (Thermo Fisher Scientific; 10888-022) medium supplemented with B-27 (2%, Thermo Fisher Scientific; 17504001), Glutamax (2 mM, Invitrogen; 35050061), and penicillin/streptomycin at 37°C in 5% CO_2 humidified incubator. To minimize potential consequences from previously reported roles of the SphK1/S1P axis or TRPC5 in neuronal development (Greka et al., 2003; Mizugishi et al., 2005; Davare et al., 2009; Puram et al., 2011), lentiviral transduction in the present study were exclusively performed in neurons at days *in vitro* (DIV)11–DIV12 when the initial wave of synaptogenesis is complete (Bassani et al., 2012; Wang et al., 2017; Ribeiro et al., 2019; Griggs et al., 2021; Nawalpuri et al., 2021); accordingly, live-cell imaging experiments were conducted on neurons at DIV16–DIV20.

Chromaffin cells in culture, prepared from adrenal glands of newborn pups with either sex as previously described (Gong et al., 2005; L. H. Yao et al., 2012, 2013), were maintained at 37°C in 5% CO_2 humidified incubator and used within 4 d for electrophysiology. Lentiviral transduction was conducted at DIV0, and cell-attached capacitance recordings was performed 72–96 h after infection.

HEK 293 cells were cultured and maintained in DMEM supplemented with 10% fetal bovine serum (FBS), 0.1 mM MEM nonessential amino acids, 6 mM L-glutamine, 1 mM MEM sodium pyruvate, 1% Pen-Strep, and 500 µg/ml Geneticin antibiotic. Cells, which typically reached 80% confluence every 3 d, were treated with trypsin-EDTA and passaged with a 1:10 ratio for the general maintenance. Cells dissociated were seeded onto 24-well culture plates and transfected with Lipofectamine LTX Reagent (Thermo Fisher Scientific; catalog #15338100), at 40–50% confluency. Transfected cells were maintained at 37°C in a 5% CO_2 humidified incubator for 48–72 h before being trypsinized and seeded to PDL-coated coverslips for whole-cell patch clamping recordings.

Cloning of DNA constructs

Plasmids containing sypHy and SynGCAMP6f were kind gifts from Dr. L. Lagnado lab (Granseth et al., 2006) and Dr. T. A. Ryan lab (de Juan-Sanz et al., 2017), respectively. The lentiviral vector pCDH-EF1-MCS-T2A-GFP was from System Biosciences. pCDH-EF1-$SphK1^{DN}$-T2A-GFP, pCDH-EF1-$SphK1^{WT}$ (N-terminal FLAG tag), pCDH-EF1-$SphK1^{DN}$ (N-terminal FLAG tag), pCDH-SYN1-sypHy and pCDH-SYN1-SynGCAMP6f were previously generated in our lab (Z.J. Jiang et al., 2019b, 2021). The protein-coding cDNA clone of mouse TRPC5, clone ID 22 067 (BC112972), was purchased from transOMIC technologies. To obtain pCDH-SYN1-$SphK1^{DN}$-T2A-sypHy or pCDH-SYN1-$SphK1^{DN}$-T2A-synGCaMP6f, $SphK1^{DN}$ was amplified by PCR, together with sypHy or synGCaMP6f, and then enzyme-digested and ligated into multiple cloning sites before and after T2A in pCDH-SYN1-MCS-T2A-MCS (a tool vector we have created in lab). Thereafter, pCDH-SYN1-$SphK1^{DN}$-T2A-synaptophysin-mCherry was created by replacing pHluorin in pCDH-SYN1-$SphK1^{DN}$-T2A-sypHy with mCherry via restriction digest and ligation. To obtain pCDH-SYN1-sypHy-T2A-$TRPC5^{DN}$, $TRPC5^{WT}$ was first amplified by PCR and then enzyme-digested and ligated between the BspEI and PmeI sites after T2A in pCDH-SYN1-sypHy-T2A-MCS, which was created previously in the lab from pCDH-SYN1-sypHy by deleting the stop codon in sypHy. $TRPC5^{DN}$ mutation (LFW-AAA; Strübing et al., 2003) was then made by QuikChange PCR (Stratagene), with pCDH-SYN1-sypHy-T2A- $TRPC5^{WT}$ as the template, thus creating pCDH-SYN1-sypHy-T2A-$TRPC5^{DN}$. Full length SphK1, TRPC5 and their mutants, together with sypHy and synGCaMP6f, amplified by PCR were verified by Sanger sequencing.

Lentiviral productions

Low-passage HEK 293 cells were co-transfected with 10 μg pCDH lentiviral vectors containing genes of interests, along with 7-μg packaging vector psPAX2 and 3 μg envelope vector pMD2.VSVG, using the polyethylenimine-mediated transfection method. The supernatant containing lentiviral particles was collected and filtered through 0.45 μm filter to remove cell debris at 48 and 72 h. Lentiviral particles, concentrated by PEG-it precipitation kits from System Bioscience, were re-suspended in cold PBS and stored at −80°C.

Drugs and reagents

Stock solutions were prepared by dissolving the following molecules: S1P (Sigma-Aldrich, catalog #S9666) at 1 mM in methanol; FTY720 (Sigma-Aldrich, catalog #SML0700) at 100 μM in ddH_2O, CAY10444 (Cayman Chemicals, catalog #10005033) at 1 mM in dimethyl formamide, and W146 (Cayman Chemicals, catalog #10009109) at 0.2 mM in methanol. Stock solutions were then diluted to final concentrations into culture medium for

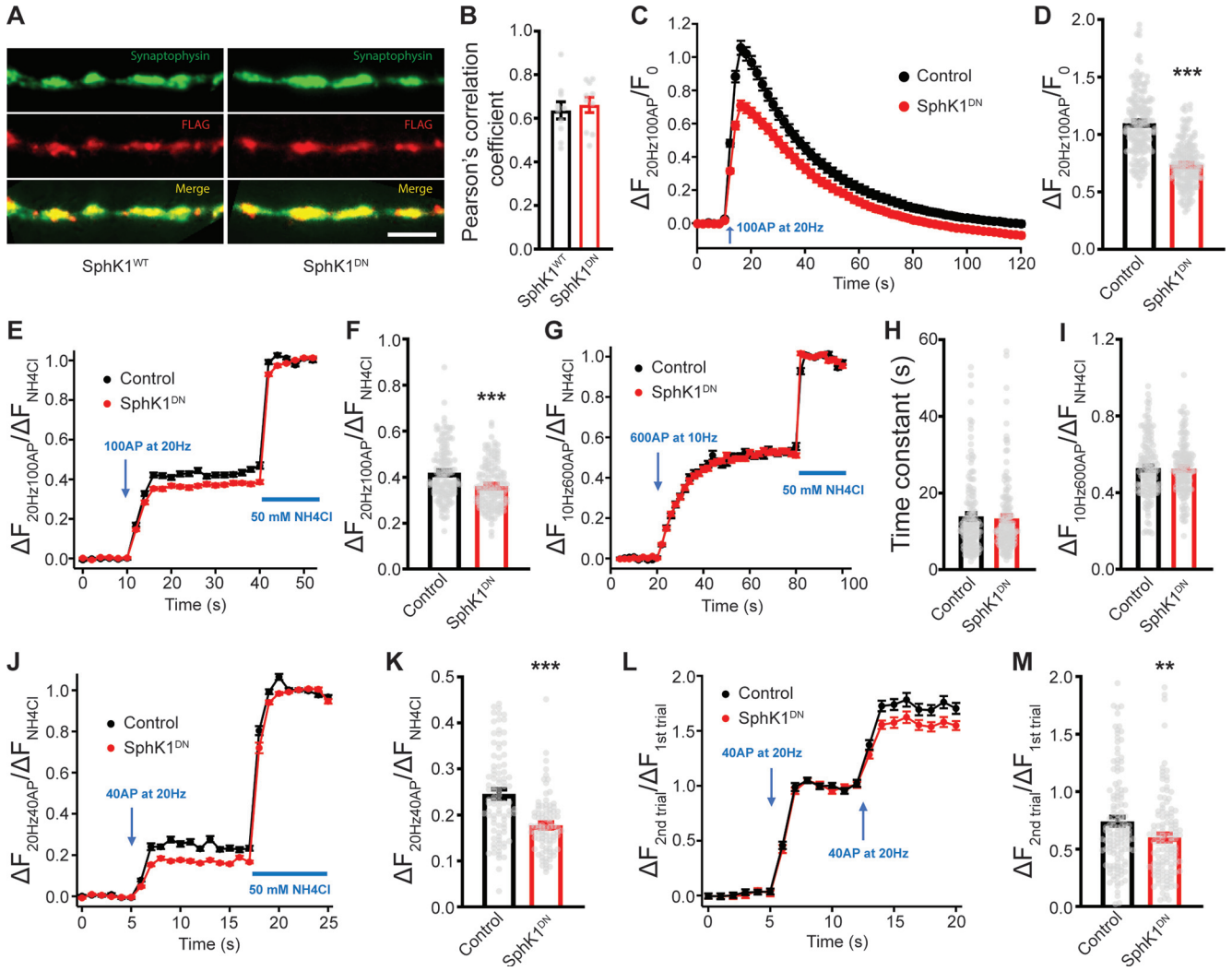

Figure 1. SphK1^{DN} inhibits RRP during exocytosis. ***A***, Representative micrographs of immunofluorescence of synaptophysin and exogenously expressed SphK1^{WT} or SphK1^{DN} show similar presynaptic localizations of these two SphK1 versions. Scale bar: 5 μm. ***B***, No significant differences in the Pearson's correlation coefficient of SphK1^{WT} or SphK1^{DN} to synaptophysin (SphK1^{WT}: $n = 10$ fields of view from 4 coverslips; SphK1^{DN}: $n = 10$ fields of view from 4 coverslips, $p = 0.6367$). ***C***, Normalized changes of sypHy fluorescence in response to a 100 APs at 20-Hz stimulation in control or SphK1^{DN}-expressing neurons. ***D***, Bar graph comparing the peak of normalized fluorescence increases in control or SphK1^{DN}-expressing neurons (control: $n = 167$ boutons; SphK1^{DN}: $n = 166$ boutons). ***E***, ***F***, In the presence of bafilomycin A1, time course (***E***) and bar graph (***F***) of increases in the sypHy signals induced by a 100 APs at 20-Hz stimulation in control or SphK1^{DN}-expressing neurons. Fluorescence increases induced by electrical stimulations are normalized to that by NH_4Cl application (control: $n = 128$ boutons; SphK1^{DN}: $n = 131$ boutons). ***G***, In the presence of bafilomycin A1, time course of normalized sypHy fluorescence increases induced by a 600 APs at 10-Hz stimulation in control and SphK1^{DN}-expressing neurons. ***H***, Bar graph showing no effects of SphK1^{DN} on the time constant of TRP depletion kinetics, which is measured by exponentially fitting sypHy increases during stimulations ($p = 0.6656$). ***I***, Bar graph showing SphK1^{DN} has no influences on TRP size ($p = 0.9057$; control: $n = 145$ boutons; SphK1^{DN}: $n = 147$ boutons). ***J***, In the presence of bafilomycin A1, time course of normalized sypHy fluorescence increases induced by a 40 APs at 20-Hz stimulation in control and SphK1^{DN}-expressing neurons. ***K***, Bar graph showing a reduction in the RRP size by SphK1^{DN} (control: $n = 89$ boutons; SphK1^{DN}: $n = 89$ boutons). ***L***, In the presence of bafilomycin A1, time course of fluorescence increases of sypHy induced by two successive 40 APs at 20-Hz stimulations with a time interval of 5 s in control and SphK1^{DN}-expressing neurons. Fluorescence changes are normalized to those induced by the first stimulation. ***M***, Bar graph showing a smaller recovery of RRP in neurons expressing SphK1^{DN} (control: $n = 129$ boutons; SphK1^{DN}: $n = 121$ boutons). $^{**}p < 0.01$ and $^{***}p < 0.001$, unpaired two-tailed Student's *t* test.

neurons, or bath solution for HEK293 cells. Neurons in culture were co-pre-incubated with CAY10444 (10 μM), a selective S1P3 antagonist, and W146 (4 μM), a selective S1P1 antagonist, for 1 h before overnight 1 nM FTY720 incubation. During electrophysiological recordings of whole-cell TRPC5 currents, 5 μM S1P is directly applied extracellularly with a pressurized local perfusion system (VC3, ALA scientific instruments) placed ~40 μm away from the patched cell.

Immunocytochemistry

Neurons in culture were fixed with 4% paraformaldehyde for 10 min at 37°C. Fixed neurons were washed twice with PBS and then permeabilized and quenched for 15 min in PBS with 0.2% saponin and 50 mM ammonium chloride at room temperature. Samples were next incubated for 1 h in blocking buffer (PBS with 5% normal donkey serum, 4% bovine serum albumin (BSA), 0.02% sodium azide (NaN_3), and 0.04% saponin) at room temperature. Primary antibodies were either diluted 1:500 (mouse anti-FLAG, clone M2, Sigma-Aldrich F1804, RRID:AB_262044) or 1:1000 (rabbit anti- synaptophysin, Synaptic Systems catalog #101002, RRID: AB_887905) in blocking buffer and incubated with neurons overnight at 4°C. Fluorescent dye-conjugated secondary antibodies (donkey anti-mouse IgG secondary antibody, Alexa Fluor 555: A-31570, RRID: AB_2536180; donkey anti-rabbit IgG secondary antibody, Alexa Fluor 488: A-21206, RRID:AB_2535792; Thermo Fisher Scientific) were diluted at 1:1000 in the blocking buffer, and incubated with cells for 1 h at room temperature. Images were collected on an Olympus IX51 microscope with a 60× oil immersion objective and captured by a Prime BSI Scientific CMOS (sCMOS) camera (Teledyne Photometrics) controlled by μManager software (https://micro-manager.org/). A Semrock TRITC-B filter cube (543/22-nm excitation, 593/40-nm emission, 562-nm dichroic mirror) was used for Alexa Fluor 555 signals, with a Semrock

GFP-3053B filter cube (473/31-nm excitation, 520/35-nm emission, 495-nm dichroic mirror) for Alexa Fluor 488 signals.

Pearson's correlation coefficient (PCC) of FLAG to synaptophysin was measured using Just Another Colocalization Plugin (JACoP) plugin in Fiji (Bolte and Cordelières, 2006). Two to three fields of view with an absence of cell bodies were randomly selected from each coverslip, and PCCs were analyzed using Costes' automatic threshold in JACoP. Data are pooled from coverslips of two independent cultures.

Live-cell imaging in neurons

Experiments were performed on an Olympus IX51 microscope with a 60× oil immersion objective at room temperature except 35–37°C in Figure 2*E*,*F*, with a GFP-3035B filter cube (472/30-nm excitation, 520/35-nm emission, 495-nm dichroic mirror; Semrock) as the filter set. Neurons on coverslips were continuously perfused at a flow rate of ~1 ml/min with bath solution (130 mM NaCl, 2.8 mM KCl, 2 mM $CaCl_2$, 1 mM $MgCl_2$, 10 mM glucose, 10 mM HEPES; pH 7.4 and ~310 mOsm). To stimulate neurons, we used Chamlide magnetic perfusion chamber (Live Cell instrument) equipped with two parallel platinum electrodes (embedded within the perfusion chamber with 7-mm spacing), which serve as field electrodes to deliver electric field stimulation at 10 V/cm with 1-ms duration to induce action potentials (APs) firing in neurons; 20 μM CNQX (Tocris Bioscience) and 50 μM D-AP5 (Tocris Bioscience) were included in the bath solution to prevent recurrent activities.

To achieve high quantum efficiency, we used the Prime BSI Scientific CMOS (sCMOS) camera (Teledyne Photometrics) controlled by μManager software (micromanager.org) for capturing images. To achieve a sampling rate of 100 Hz for experiments of single AP stimulations and minimize photobleaching for experiments of train stimulations, the electrical stimulation via a programmable isolated high-powered stimulator (AM Systems, Model 4100), illumination via λ 421 Optical Beam Combining System (Sutter Instruments) and data acquisition via camera were simultaneously controlled by TTL output signals via Igor software (RRID: SCR_000325, WaveMetrics). For Ca^{2+} imaging experiments using SynGCaMP6f, the light intensity of illumination was set at 40% in combination with a 10-ms exposure time for single AP experiments stimulation or 20% in combination with a 100-ms exposure time for train stimulations. Images were captured at a 1- or 2-s interval with 100-ms exposure time at 20% illumination during sypHy experiments.

To measure reacidification rate of newly formed endocytic vesicles using sypHy as described previously (Z.J. Jiang et al., 2021), neurons on coverslip were rapidly superfused with a valve controlled pressurized perfusion system (ALA Scientific). The perfusing buffer was switched between the standard pH 7.3 bath solution described above and pH 5.5 buffer with the HEPES substituted with equimolar MES, with electrical stimulation time-locked to frame acquisition and buffer changes. Specifically, surface fluorescence of pHluorin is quenched by the first application of acidic buffer (pH 5.5) for 6s to establish the baseline, and the quenched fluorescence is recovered by washing off the acidic solution. To isolate pHluorin signal from newly endocytosed SVs, acidic buffer (pH 5.5) is applied for a 30-s duration 2 s right after the cessation of stimulation train. Newly endocytosed alkaline pool of pHluorin is detached from the plasma membrane and thus resistant to quenching by the applied acidic buffer, and the decay of this portion of fluorescence to the baseline represents acidification of newly endocytosed vesicles. Therefore, reacidification rate of newly endocytosed vesicles is estimated by an exponential fit of the fluorescent signal decay from the first to the last point during the 30-s duration of acidic buffer application.

To measure vesicles exocytosis as previously described (Balaji and Ryan, 2007; Baumgart et al., 2015), boutons were stimulated in the presence or absence of 1 μM bafilomycin A1 (Cayman, catalog #11038), which eliminated interference of endocytosis by blocking reacidification of endocytosed vesicles. Tyrode's solution containing 50 mM NH_4Cl were perfused at the end of each test to collapse the pH gradient across vesicle membrane thus revealing the total pool.

Image analysis

Images from sypHy experiments were analyzed in ImageJ (RRID: SCR_000415; http://rsb.info.nih.gov/ij) using custom-written plugins (http://

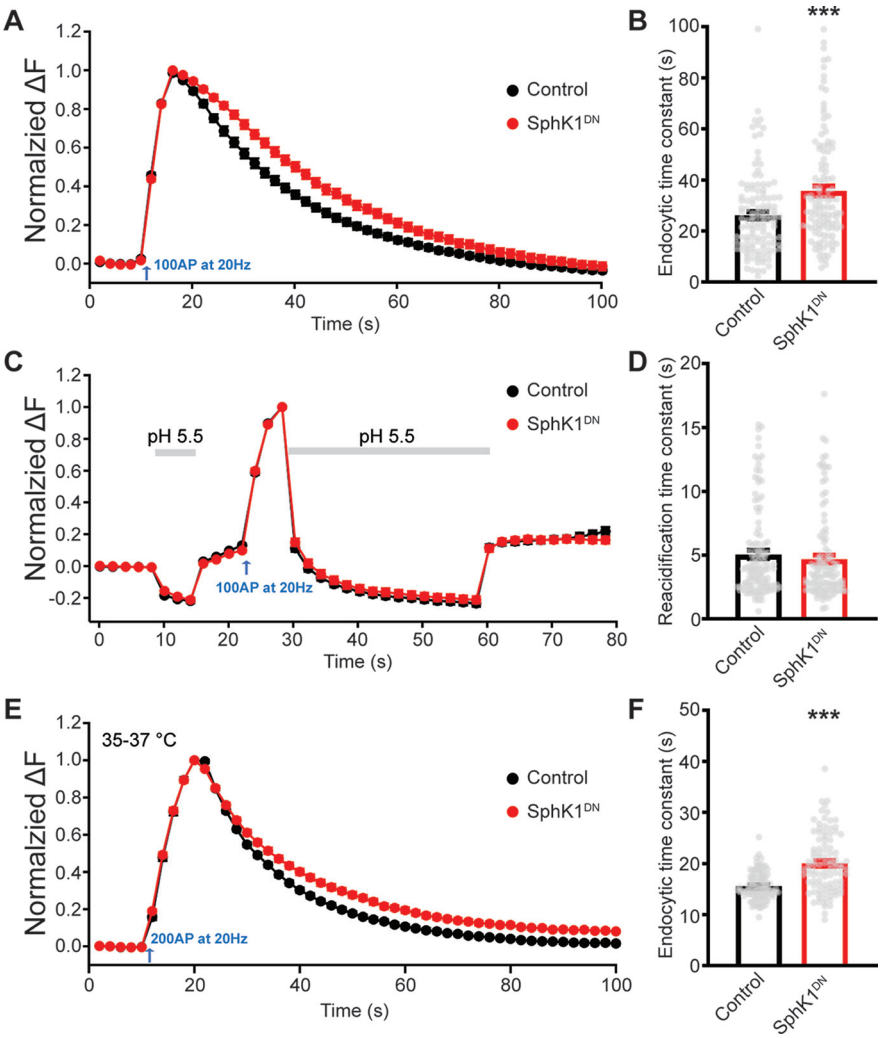

Figure 2. Synaptic vesicle endocytosis is impaired in $SphK1^{DN}$-expressing neurons. ***A***, Normalized fluorescence changes of sypHy signals in control and $SphK1^{DN}$-expressing neurons. ***B***, Bar graph showing an increase in the endocytic time constant by $SphK1^{DN}$ (control: $n = 121$ boutons; $SphK1^{DN}$: $n = 117$ boutons). ***C***, Normalized sypHy signals with two perfusion periods with pH 5.5 MES buffer as indicated in the trace (gray bars). Newly endocytosed vesicles "trapped" during acidic buffer perfusion starting 2 s after 100 APs at 20 Hz. ***D***, Bar graph comparing the reacidification rate of endocytic vesicles, which was obtained by exponential fittings of fluorescence decay, indicates no change in this parameter by $SphK1^{DN}$ (control: $n = 117$ boutons; $SphK1^{DN}$: $n = 115$ boutons, $p = 0.4198$). ***E***, Normalized changes of sypHy signals in control and $SphK1^{DN}$-expressing neurons at 35–37°C. ***F***, Bar graph comparing the endocytic time constant shows an increase in the endocytic time constant induced by $SphK1^{DN}$ at physiological temperature (control: $n = 101$ boutons; $SphK1^{DN}$: $n = 100$ boutons). ***$p < 0.001$, unpaired two-tailed Student's t test.

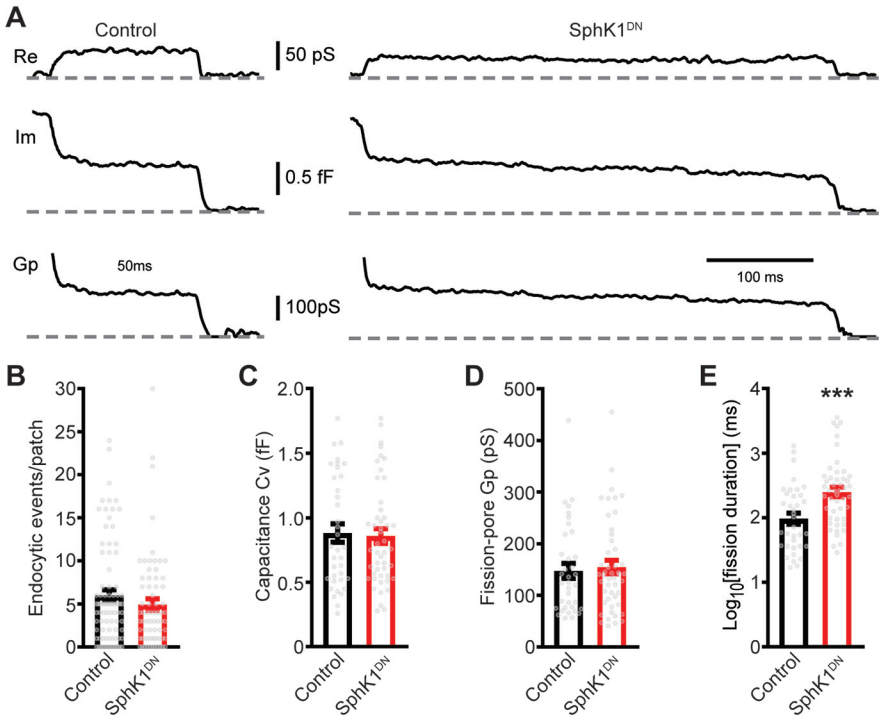

Figure 3. SphK1^{DN} slows down vesicle fission during endocytosis in neuroendocrine chromaffin cells. ***A***, Representative endocytic events, as membrane conductance (Re), membrane capacitance (Im) and the fission-pore conductance (Gp), in control and SphK1^{DN}-expressing cells. ***B–E***, The number of endocytic events (control: $n = 83$ cells; SphK1^{DN}: $n = 69$ cells, $p = 0.2501$; ***B***), the capacitance Cv of endocytic vesicles ($p = 0.8041$; ***C***), and the fission-pore Gp ($p = 0.7110$; ***D***) were statistically comparable between control and SphK1^{DN}-expressing cells; the log transformed fission-pore duration (***E***) was significantly increased in SphK1^{DN}-expressing cells (control: $n = 36$ events; SphK1^{DN}: $n = 48$ events). ***$p < 0.001$, unpaired two-tailed Student's *t* test.

rsb.info.nih.gov/ij/plugins/time-series.html) and Igor software using custom-written procedures. Photobleaching was <2% for all images included in our analysis and thus was not corrected. To analyze images from sypHy experiments, regions of interest (ROIs) of identical size (4 × 4 pixels) were placed in the center of individual synaptic boutons reacting to stimuli, and fluorescence changes were tracked throughout the image stack. In general, 10–25 ROIs were analyzed from each coverslip for sypHy experiments. With Igor, fluorescent intensities of individual ROIs before stimuli were averaged as baseline (F0), the fluorescent changes (ΔF) were normalized to the baseline (F0) as ΔF/F0 or the fluorescence changes induced by NH_4Cl (ΔF_{NH4Cl}) as $\Delta F/\Delta F_{NH4Cl}$ for exocytosis, or to the peak of fluorescent increase (ΔFmax) as ΔF/ΔFmax for endocytosis. Normalized ΔF of individual ROIs were taken as independent replicates (n) for each sypHy experiment, acquired from 7–12 coverslips of two to four cultures.

To analyze data for SynGCaMP6f experiments, ROIs were created as previously reported in Fiji (https://fiji.sc/; Vevea and Chapman, 2020; Z. J. Jiang et al., 2021). Briefly, ROIs (>10 pixels), defined by a series of image subtractions and thresholding, were used to measure fluorescence changes of image stacks. Next, fluorescent intensities of individual ROIs before stimuli were averaged as baseline (F0), and the fluorescent changes (ΔF) were normalized to the baseline (F0) as ΔF/F0 in Igor. The independent replicates (n) for each SynGCaMP6f study, pooled from two to four cultures, was measured as the average of normalized ΔF of all ROIs from each coverslip.

Cell-attached capacitance recordings and analyses of endocytic fission-pore

Cell-attached capacitance recordings of membrane capacitance and conductance were performed as described previously (L.H. Yao et al., 2012, 2013). Fire polished pipettes had a typical resistance of ~2 megaohms in the bath solution. The bath solution contained 130 mM NaCl, 5 mM KCl, 2 mM $CaCl_2$, 1 mM $MgCl_2$, 10 mM HEPES-NaOH, and 10 mM HEPES-NaOH; the pH was adjusted to 7.3 with NaOH. As mentioned previously (L.H. Yao et al., 2012, 2013), capacitance steps and fission-pore durations were considered as reliably detected for step sizes >0.2 fF, and smaller capacitance steps are not included in the analysis. Endocytic events were recorded right after gigaseal formation, since we often detected action currents in the membrane current trace as shown previously (Dernick et al., 2005), which indicates firing of action potentials likely induced by mechanic stimulus of patching in chromaffin cells. The number of endocytic events per patch detected in the cell-attached recordings is counted as the total number of downward capacitance steps within the first 5 min of recordings (L.H. Yao et al., 2012, 2013). The fission-pore Gp for endocytic events was calculated as $Gp_{(Im)} = \frac{\omega \cdot Cv}{\sqrt{\left(\frac{\omega \cdot Cv}{Im}\right)-1}}$ (Gong et al., 2005; L.H. Yao et al., 2012, 2013). The fission-pore duration was defined as the time interval from the first point where Gp decreased below 2 nS and the final drop in Gp to zero. This final drop reflects the step response of the low pass filter setting of the lock-in amplifier (1 ms, 24 dB). At this setting, 90% of the final value is reached within ~7 ms, so the last point of the fission-pore was taken as the time at 7–10 ms before the final drop to zero in the Gp trace. The fission-pore conductance Gp was taken as the average Gp value during the fission-pore duration time interval. Analysis of fission-pore kinetics were restricted to fission-pores with durations >15 ms, since shorter events were distorted by the lock-in amplifier low-pass filter (set to 1 ms, 24 dB; L.H. Yao et al., 2012, 2013). Data are pooled from coverslips of four independent cultures.

Whole-cell recordings of TRPC5 currents in HEK 293 cells

TRPC5 currents were monitored in HEK 293 cells using the whole-cell configuration as previously reported (Xu et al., 2006; Gomis et al., 2008; Blair et al., 2009). The bath solution contained 130 mM NaCl, 5 mM KCl, 2 mM $CaCl_2$, 1 mM $MgCl_2$, 10 mM HEPES-NaOH, and 10 mM glucose; the pH was adjusted to 7.3 with NaOH, and the osmolarity was ~310 mmol/kg. The solution in the whole-cell pipette contained 130 mM Cs-$MeSO_3$, 5 mM Na_2ATP, 0.1 mM Na_3GTP, 2 mM $MgCl_2$, 1.3 mM $CaCl_2$, 2 mM EGTA-CsOH, and 10 mM HEPES; the pH was adjusted to 7.3 with CsOH, and the osmolarity was adjusted to 290 mmol/kg. The voltage ramp protocol holds cells at −60 mV, steps to −100 mV for 40 ms, and then ramps to +100 mV over 500 ms, holding at +100 mV for 40 ms before stepping back to −60 mV, and this protocol is repeated every 5 s during recordings. Series resistance was monitored by applying a voltage step of 10 mV. Current signals were filtered at 3 kHz and digitized at 20 kHz. Only recordings with an initial pipette-membrane seal resistance >2 GΩ were included. Current traces and time courses were analyzed with customized macro for Igor software.

Statistical analysis

Data were tested for normal distribution and, if necessary, log-transformed for the fission-pore duration in Figures 3*E* to fulfill the criteria of normal distributions for Student's *t* tests. All statistical analyses were performed with Prism (RRID: SCR_002798, GraphPad).

No statistical method was used to predetermine sample size, but our samples sizes are comparable to those reported in previous studies (Fernández-Alfonso and Ryan, 2004; Granseth et al., 2006; L.H. Yao et al., 2012, 2013; Soykan et al., 2017; Z.J. Jiang et al., 2021). Cells were randomly assigned into control or experimental groups, and data were

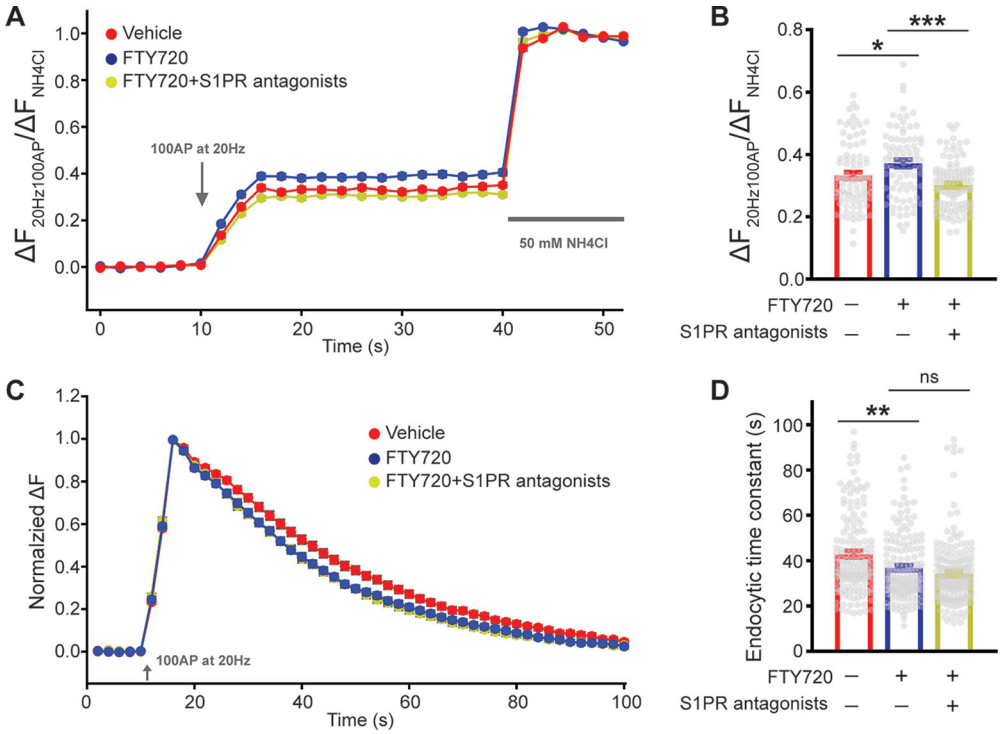

Figure 4. S1P1/S1P3 receptors are critical for the FTY720-mediated rescue on synaptic vesicle exocytosis but not endocytosis in SphK1^{DN}-expressing neurons. ***A***, In the presence of bafilomycin A1, synaptic vesicle exocytosis induced by electrical stimulations was measured by normalizing the fluorescence increase induced by electrical stimulation to that by NH_4Cl perfusion in SphK1^{DN}-expressing neurons under variable conditions (control, FTY720, or FTY720/W146/CAY10444). FTY720 is a clinical S1P analog; W146 and CAY10444 are specific antagonists for S1P1 and S1P3 receptors, respectively. ***B***, Bar graph comparing synaptic vesicle exocytosis in SphK1^{DN}-expressing neurons between these three groups as shown in ***A*** (control: $n = 95$ boutons; FTY720: $n = 85$ boutons; FTY720 and S1PR antagonists: $n = 106$ boutons). One-way ANOVA followed by Tukey's *post hoc* test: FTY720 versus control (*$p < 0.05$); FTY720 and S1PR antagonists versus FTY720 (***$p < 0.001$). ***C***, Normalized changes of sypHy signals in SphK1^{DN}-expressing neurons under different conditions (control, FTY720, or FTY720 and S1P1/S1P3 inhibitors). ***D***, Bar graph comparing the endocytic time constant in SphK1^{DN}-expressing neurons shows that FTY720 treatment accelerates synaptic vesicle endocytosis independent of S1PR inhibitors (control: $n = 162$ boutons; FTY720: $n = 159$ boutons; FTY720 and S1PR inhibitors: $n = 178$ boutons). One-way ANOVA followed by Tukey's *post hoc* test: FTY720 versus control (**$p < 0.01$); FTY720 and S1PR inhibitors versus FTY720 ($p = 0.2759$; ns: not statistically significant).

expressed as mean ± SEM, with all values from quantification plotted as gray dots in the bar graph. Statistical analysis was performed with unpaired two-tailed Student's *t* test, except paired two-tailed Student's *t* test in Figure 8*H* and Newman of one-way ANOVA in Figures 4*B*,*D*, 7*B*, and 8*B*. All analyses were performed by an investigator blinded to the experimental condition. *N* numbers, full statistics, and *p* values were reported and listed in the related figure legends and Extended Data Table 1-1.

Results

SphK1^{DN} inhibits the readily release Pool (RRP) during exocytosis in neurons

SphK1, a kinase essential for S1P production in central nervous system, is concentrated within presynaptic terminals in neurons (Fukuda et al., 2003; Kajimoto et al., 2007; Bryan et al., 2008; Chan et al., 2012). A dominant-negative mutant, SphK1^{DN} (G82D) is reported to significantly inhibit S1P production (Lan et al., 2011; Pitson et al., 2002; Qi et al., 2015). In neuroendocrine chromaffin cells, we have previously demonstrated that down-regulation of S1P production by SphK1^{DN} induces significant defects in vesicle exocytosis (Z.J. Jiang et al., 2019b). In neurons, SphK1^{DN} expressed by lentivirus displays a similar presynaptic localization as wild-type (WT) SphK1 (SphK1^{WT}; Fig. 1*A*,*B*), which is not surprising as this SphK1^{DN} mutant only harbors a single amino acid substitution in its kinase catalytic domain (Pitson et al., 2000; Alemany et al., 2007). We next analyzed effects of SphK1^{DN} on synaptic vesicle recycling in cortical neuron cultures using sypHy (Granseth and Lagnado, 2008; Royle et al., 2008). SphK1^{DN} significantly reduced the fluorescence increase of sypHy signals induced by 100 APs at 20-Hz stimulations ($p < 0.001$; Fig. 1*C*,*D*), indicating a role of SphK1 in synaptic vesicle exocytosis. It is aware that such an increase in sypHy fluorescence likely represents a net outcome of synaptic vesicle exocytosis and endocytosis (Fernández-Alfonso and Ryan, 2004; Voglmaier et al., 2006). To eliminate any interference of endocytic signals, the increase in sypHy signals during stimulations were measured in the presence of the H^+ ATPase inhibitor bafilomycin A1 (Granseth et al., 2006; Z.J. Jiang et al., 2021). To our expectation, the increase of sypHy signals was also inhibited by SphK1^{DN} under this condition, thus confirming a role of SphK1 kinase activity in synaptic vesicle exocytosis ($p < 0.001$; Fig. 1*E*,*F*).

We next determined effects of SphK1^{DN} on the total recycling pool (TRP) and readily releasable pool (RRP), two pools that are essential in determining the amount of synaptic vesicle exocytosis (S.H. Kim and Ryan, 2010; Alabi and Tsien, 2012; Baumgart et al., 2015). As reported previously, TRP was evaluated as fluorescence increases of sypHy in response to stimulations of 600 APs at 10 Hz (Fig. 1*G*; Ryan and Smith, 1995; Z. Hua et al., 2011). Our results showed that SphK1^{DN} did not alter either the size or the depletion kinetics of TRP ($p > 0.05$; Fig. 1*H*,*I*). On the other hand, RRP was evaluated as sypHy increases in response to 40 APs at 20-Hz stimulation (Fig. 1*J*; Murthy and Stevens, 1999; Schikorski and Stevens, 2001; Li et al., 2005; Granseth et al., 2006; Granseth and Lagnado, 2008). Additionally, the replenishment of RRP was estimated as fluorescent increase induced by

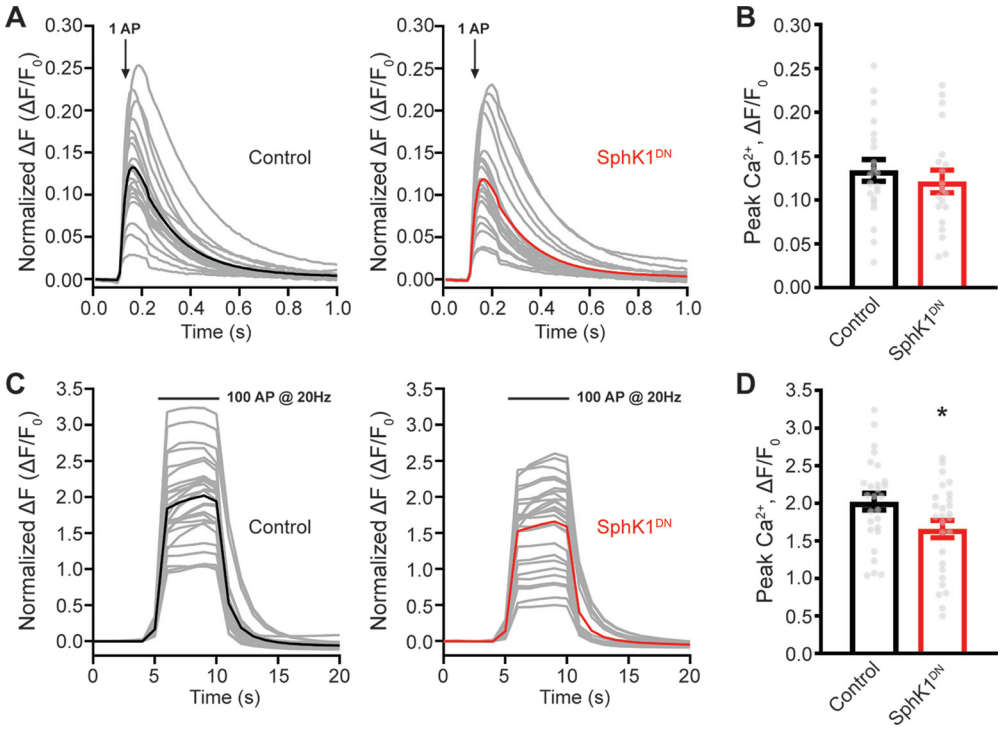

Figure 5. SphK1^{DN} impairs presynaptic Ca^{2+} increase in response to prolonged stimulations rather than single AP stimulation. ***A***, Normalized synGCaMP6f increases induced by single AP in control or SphK1^{DN}-expressing neurons. Gray lines are mean fluorescence changes of individual ROIs from each coverslip, with black and red line as the averaged response of individual coverslips in control and SphK1^{DN} group, respectively. Raw data for Ca^{2+} increases induced by single AP are presented in Figure 6. ***B***, Bar graph comparing peak synGCaMP6f values as shown in **A** reveals no change in Ca^{2+} signals by SphK1^{DN} (control: $n = 21$ coverslips; SphK1^{DN}: $n = 20$ coverslips, $p = 0.4865$). ***C***, Normalized synGCaMP6f increases induced by 100 APs at 20-Hz stimulations in control or SphK1^{DN}-expressing neurons. Gray lines are mean fluorescence changes of individual ROIs from each coverslip, with black and red line as the averaged response of individual coverslips in control and SphK1^{DN} group, respectively. ***D***, Bar graph comparing peak synGCaMP6f values as shown in **C** demonstrates a defective Ca^{2+} signals by SphK1^{DN} (control: $n = 27$ coverslips; SphK1^{DN}: $n = 27$ coverslips). In addition, this SphK1^{DN}-induced presynaptic Ca^{2+} reductions can be rescued by FTY720 application, independent of S1P1/S1P3 receptors (Fig. 7). *$p < 0.05$, unpaired two-tailed Student's *t* test.

the second 40 APs at 20-Hz stimulation 5 s after RRP depletion by the first 40 APs at 20-Hz stimulation, as described previously (Granseth and Lagnado, 2008). SphK1^{DN} significantly reduced RRP size ($p < 0.001$; Fig. 1*J*,*K*) and slowed down RRP replenishment ($p < 0.01$; Fig. 1*L*,*M*). Collectively, this set of experiments indicate that SphK1 kinase activity may be critical for synaptic vesicle exocytosis by regulating RRP rather than TRP within presynaptic terminals.

SphK1^{DN} slows down synaptic vesicle endocytosis in neurons

To determine any potential roles of the SphK1/S1P axis in synaptic vesicle endocytosis, we examined effects of SphK1^{DN} on the decay kinetics of sypHy signals on the cessation of stimulations (Fig. 2*A*). SphK1^{DN} substantially increased the time constant of sypHy fluorescence decay ($p < 0.001$; Fig. 2*B*), with no alternation in the reacidification kinetics of newly formed endocytic vesicles ($p > 0.05$; Fig. 2*C*,*D*), indicating an importance of SphK1 kinase activity in synaptic vesicle endocytosis. In addition, we observed an increase in the endocytic time constant induced by SphK1^{DN} at the physiological temperature of 35–37°C ($p < 0.001$; Fig. 2*E*,*F*), thus reiterating an importance of SphK1 kinase activity in synaptic vesicle endocytosis in neurons.

SphK1^{DN} prolongs fission-pore duration during endocytosis in chromaffin cells

To understand whether the SphK1/S1P axis is involved in the modulation of vesicle fission, a critical and arguably rate limiting step during endocytosis (Haucke et al., 2011; Saheki and De Camilli, 2012; Kononenko and Haucke, 2015; Kaksonen and Roux, 2018), we analyzed effects of SphK1^{DN} on the fission-pore kinetics in neuroendocrine chromaffin cells by monitoring single vesicle endocytosis with cell-attached capacitance recordings as described previously (Fig. 3*A*; L.H. Yao et al., 2012; Varga et al., 2020; Z.J. Jiang et al., 2021). SphK1^{DN} induced a 17.8% reduction in the number of endocytic events, although this reduction was not significant (Fig. 3*B*). Meanwhile, the capacitance size of endocytic vesicles was comparable between these two groups (Fig. 3*C*), indicating that SphK1 may not be critical in controlling the size of endocytic vesicles. Additionally, SphK1^{DN} had no obvious effect on the fission-pore conductance (Gp; Fig. 3*D*), implying that SphK1 may not be essential in determining the geometry of the tubular membrane neck during endocytosis. However, SphK1^{DN} significantly increased the fission-pore duration ($p < 0.001$; Fig. 3*E*), indicating an essential role of SphK1 kinase activity in vesicle fission during endocytosis.

S1P receptors are crucial for the SphK1/S1P axis-mediated actions in synaptic vesicle exocytosis but not endocytosis

FTY720, a clinical oral treatment of relapsing remittent multiple sclerosis (Chiba and Adachi, 2012; Ali et al., 2013), is a synthetic S1P analog (Nofer et al., 2007). We thus examined whether FTY720 could rescue exocytic and endocytic defects of synaptic vesicles induced by SphK1^{DN}. Neurons in culture expressing SphK1^{DN} were incubated with FTY720 at a low concentration of 1 nM overnight to mimic *in vivo* applications in animals (Stessin et al., 2012; Di Menna et al., 2013; Zhang et al., 2017). FTY720 treatments significantly enhanced the fluorescence increase of

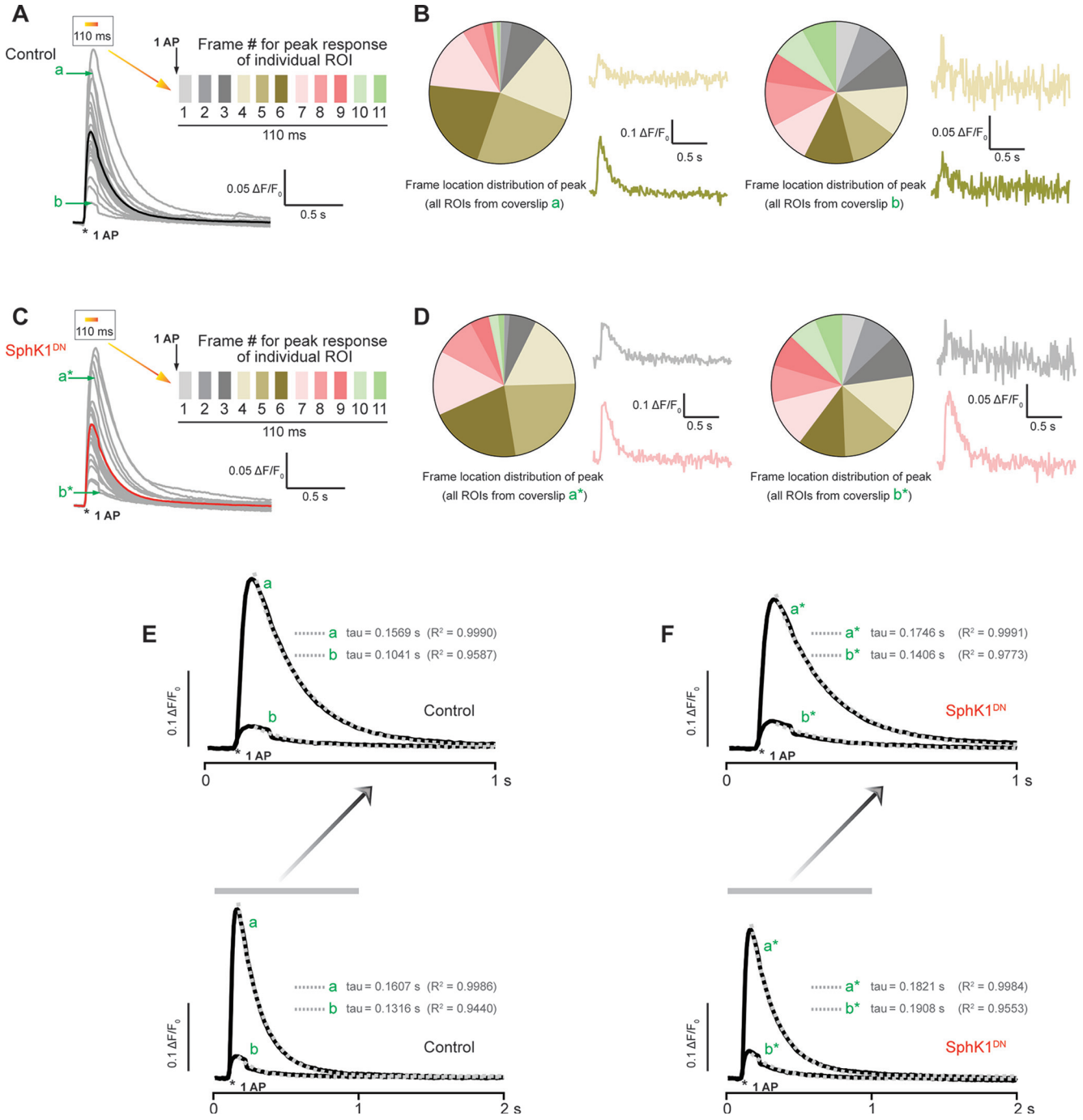

Figure 6. Raw data for Ca^{2+} increases induced by single AP in control and $SphK1^{DN}$-expressing neurons. ***A***, Time courses of normalized synGCaMP6f increases induced by single AP in control neurons. Gray lines are mean fluorescence changes of individual ROIs from each coverslip, with the black line as the averaged response of individual coverslips. As shown on top of the traces, peak Ca^{2+} signal induced by 1 AP from individual ROIs occurred within 110 ms, ranging from the first to 11th frame after stimulus as shown with color coded diagram (upper right). ***B***, Color coded pie charts showing frame location distributions of Ca^{2+} peaks for all ROIs in coverslips "a" (left) and "b" (right). Along with each pie chart, two color coded traces from each coverslip showed representative ROIs with Ca^{2+} peaked at the fourth and sixth frame. ***C***, Time courses of normalized synGCaMP6f increases induced by single AP in $SphK1^{DN}$-expressing neurons. Gray lines are mean fluorescence changes of individual ROIs from each coverslip, with the red line as the averaged response of individual coverslips. As shown on top of the traces, peak Ca^{2+} signal induced by 1 AP from individual ROIs occurred within 110 ms, ranging from the first to 11th frame after stimulus as shown with color coded diagram (upper right). ***D***, Color coded pie charts showing frame location distributions of Ca^{2+} peaks from all ROIs in coverslips "a*" (left) and "b*" (right) from $SphK1^{DN}$ group. Along with each pie chart, two color coded traces from each coverslip showed representative ROIs with Ca^{2+} peaked at the second and seventh frame. ***E***, Truncated (above) and full (below) time courses of mean synGCaMP6f signals induced by single AP of coverslip "a" or "b" from control group, with decay phases fitted by single exponential functions (dotted gray lines). ***F***, Truncated (above) and full (below) time courses of mean synGCaMP6f signals induced by single AP of coverslip "a*" or "b*" from $SphK1^{DN}$ group, with decay phases of each mean Ca^{2+} signal fitted by single exponential functions (dotted gray lines).

sypHy in response to 100 APs at 20-Hz stimulations (Fig. 4*A*,*B*) and reduced the endocytic time constant of sypHy signal decay after the cessation of stimulations (Fig. 4*C*,*D*), suggesting that FTY720 may be capable of rescuing $SphK1^{DN}$ induced exocytic and endocytic defects in neurons. These data emphasize an importance of S1P in $SphK1^{DN}$-mediated actions in synaptic vesicle exocytosis and endocytosis, thus emphasizing critical roles of the SphK1/S1P axis in synaptic vesicle recycling within presynaptic

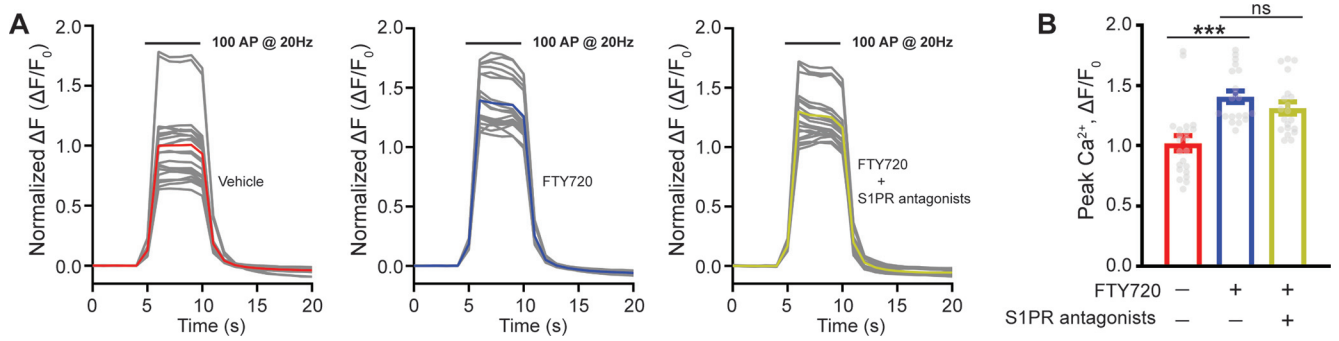

Figure 7. FTY720 rescues presynaptic Ca^{2+} increase in response to prolonged stimulations in $SphK1^{DN}$-expressing neurons, independent of S1P1/S1P3 receptors. ***A***, Normalized synGCaMP6f increases induced by 100 APs at 20-Hz stimulations in $SphK1^{DN}$-expressing neurons under variable conditions (control, FTY720, or FTY720/W146/CAY10444). Gray lines are mean fluorescence changes of individual ROIs from each coverslip, with red, blue, and yellow line as the averaged response of individual coverslips from control, FTY720, and FTY720/W146/CAY10444 group, respectively. ***B***, Bar graph comparing peak synGCaMP6f values as shown in ***A*** demonstrates that FTY720 treatment increases Ca^{2+} influx in $SphK1^{DN}$-expressing neurons, which is not affected by the pretreatment of S1PR inhibitors (control: $n = 22$ coverslips; FTY720: $n = 20$ coverslips; FTY720/W146/CAY10444: $n = 20$ coverslips). All experiments are performed in synapses expressing the $SphK1^{DN}$ mutant, one-way ANOVA followed by Tukey's *post hoc* test: FTY720 versus control (***$p < 0.001$); FTY720 and S1PR inhibitors versus FTY720 ($p = 0.4651$; ns: not statistically significant).

terminals. Notably, it has been reported that the S1P-induced effect on synaptic transmission at presynaptic terminals is mostly mediated through activation of S1P3 and/or S1P1 receptors (Kajimoto et al., 2007; Sim-Selley et al., 2009; Kanno and Nishizaki, 2011; Riganti et al., 2016; Willems et al., 2016). Hence, we next examined whether co-preincubations of W146, a specific S1P1 receptor inhibitor (Sanna et al., 2006; Ammar et al., 2013; Riganti et al., 2016), and CAY10444, a specific S1P3 receptor inhibitor (Koide et al., 2002; Pyne and Pyne, 2011; Riganti et al., 2016), would be able to block FTY720-mediated rescues we have observed. W146 and CAY10444 treatments indeed abolished FTY720-mediated rescue on the increase of sypHy fluorescence induced by stimulations (Fig. 4*A*,*B*), suggesting that S1P1/S1P3 receptors may mediate the role of the SphK1/S1P axis in synaptic vesicle exocytosis. On the other hand, treatments with W146 and CAY10444 had no detectable effects on the FTY720-mediated rescue on the endocytic time constant on the cessation of stimulations (Fig. 4*C*,*D*), indicating that S1P1/S1P3 receptors may be dispensable for the regulation of the SphK1/S1P axis in synaptic vesicle endocytosis.

The SphK1/S1P axis is important for presynaptic Ca^{2+} levels during prolonged stimulations

Previous studies in non-neuronal cells have implied important roles of S1P in modulating intracellular Ca^{2+} signaling (Ghosh et al., 1990; Itagaki and Hauser, 2003; Spiegel and Milstien, 2003; Xu et al., 2006). Since Ca^{2+} is a key regulating factor for synaptic vesicle endocytosis (Cousin, 2000; Wu et al., 2009; Wu and Wu, 2014; Chanaday et al., 2019; Z.J. Jiang et al., 2021), it is possible that a regulation of presynaptic Ca^{2+} signaling may account for the action of the SphK1/S1P axis in synaptic vesicle endocytosis we have observed. To test this possibility, we examined effects of $SphK1^{DN}$ on presynaptic Ca^{2+} signaling using synGCaMP6f (GCaMP6f fused with synaptophysin), a presynaptic Ca^{2+} reporter with fast speed and high sensitivity (Chen et al., 2013; Kyung et al., 2017; Brockhaus et al., 2019; Z.J. Jiang et al., 2021). $SphK1^{DN}$ did not alter the increase of synGCaMP6f signals induced by single AP stimulation (Fig. 5*A*,*B*; $p > 0.05$), indicative of no change in Ca^{2+} influx via VGCCs (S.H. Kim and Ryan, 2013; Brockhaus et al., 2019; Z.J. Jiang et al., 2021). It should be noted that a deflection of the SynGCaMP6f fluorescence signal was observed in the decay phase at around 110 ms following single AP stimulation (Fig. 5*A*). We suggest that this deflection may be because of, but not limited to, that single AP fluorescence responses of individual ROIs peak within the 110-ms period after stimulus, with variability in the time of the signal to peak (Fig. 6*A–D*), and its presence has no impact on the exponential decay of the averaged fluorescent signal (Fig. 6*E*,*F*). On the other hand, the increase in synGCaMP6f signals induced by 100 APs at 20-Hz stimulations was significantly reduced by $SphK1^{DN}$ ($p < 0.05$; Fig. 5*C*,*D*), suggesting an importance of the SphK1/S1P axis in regulating presynaptic Ca^{2+} influx during prolonged stimulations. This conclusion is further supported by our observation that FTY720 enhanced the increase in synGCaMP6f signals induced by 100 APs at 20-Hz stimulations in $SphK1^{DN}$-expressing neurons ($p < 0.001$), which is independent of S1P1/S1P3 receptors (Fig. 7). Presynaptic Ca^{2+} influx on prolonged stimulations has been well documented to be essential for synaptic vesicle endocytosis (C.K. Yao et al., 2009, 2017; Wu and Wu, 2014; Z.J. Jiang et al., 2021), our data thus indicate that the SphK1/S1P axis may regulate synaptic vesicle endocytosis by modulating presynaptic Ca^{2+} levels during prolonged stimulations.

S1P modulates presynaptic Ca^{2+} levels via TRPC5 channels

It is reported that the TRPC5 channel, a Ca^{2+} permeable member of canonical transient receptor potential channel (TRPC) superfamily (Clapham, 2003; Venkatachalam and Montell, 2007), is located to presynaptic terminals (Greka et al., 2003; Nichols et al., 2007; Schwarz et al., 2019). Additionally, TRPC5 channels may be involved in maintaining presynaptic Ca^{2+} levels during stimulation trains (Schwarz et al., 2019). Notably, S1P is a physiological agonist for Ca^{2+} influx via TRPC5 channels (Xu et al., 2006; Venkatachalam and Montell, 2007; Naylor et al., 2016). It is therefore possible that the regulation of TRPC5 by the SphK1/S1P axis may account for the $SphK1^{DN}$ induced presynaptic Ca^{2+} defect during prolonged stimulations we have observed (Fig. 5*C*,*D*). We next explored this possibility by examining effects of $SphK1^{DN}$ on presynaptic Ca^{2+} levels in neurons expressing a dominant negative nonconducting TRPC5 ($TRPC5^{DN}$), which was created by site-specific mutagenesis of WT TRPC5 ($TRPC5^{WT}$; LFW-AAA) as reported (Greka et al., 2003). The nonconducting and dominant negative properties of this $TRPC5^{DN}$ channel was confirmed by whole-cell patch recordings in HEK 293 cells (Fig. 8*A*,*B*). Furthermore, ionic currents of $TRPC^{WT}$ channels were significantly

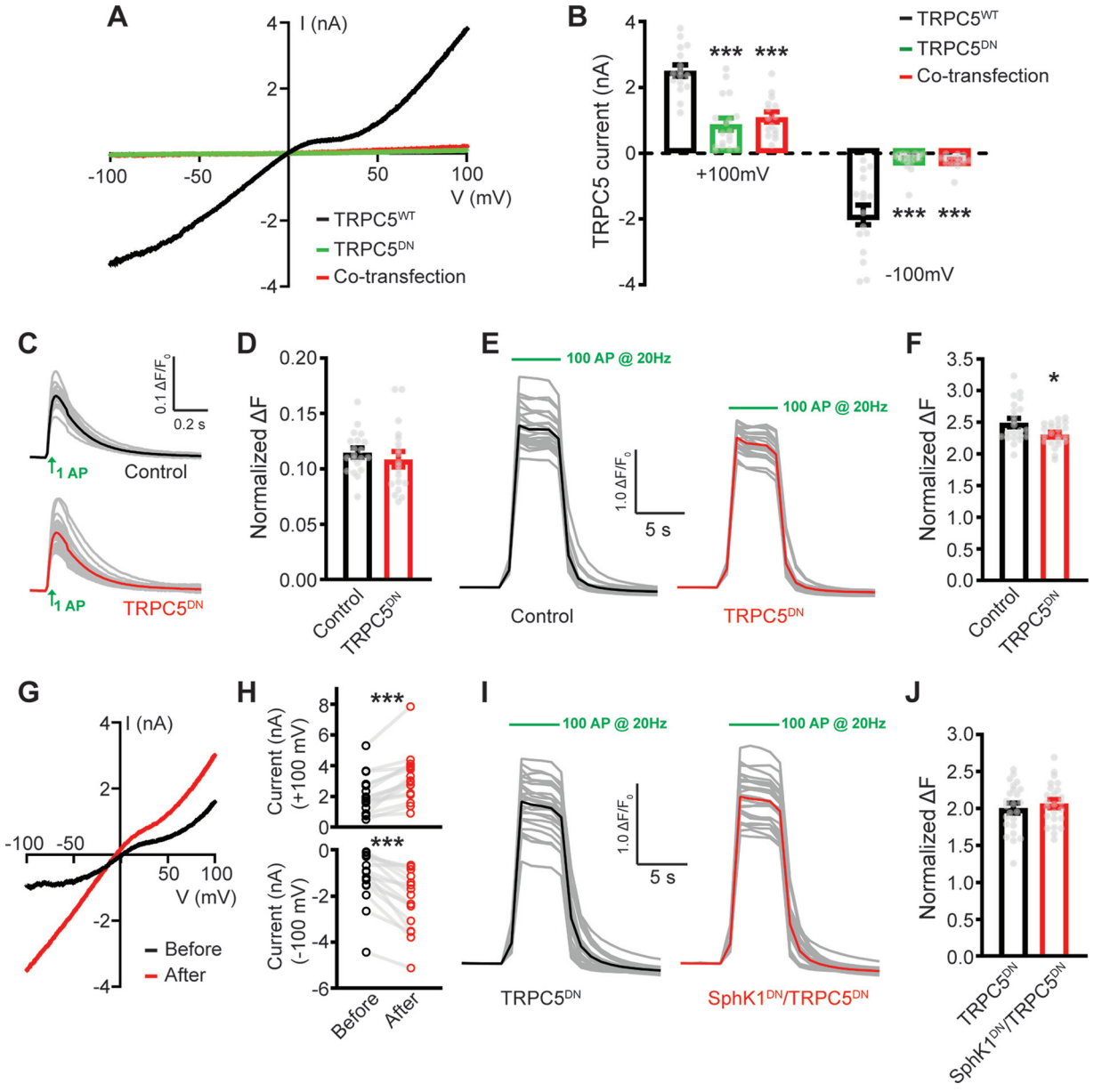

Figure 8. Ca^{2+} influx via TRPC5 is necessary for the action of the SphK1/S1P axis on presynaptic Ca^{2+} levels in responses to prolonged stimulations. ***A***, Representative whole-cell currents recorded in HEK293 cells expressing $TRPC5^{WT}$ (black), $TRPC5^{DN}$ (green), or $TRPC5^{DN}$ and $TRPC5^{WT}$ (red), in response to a voltage ramp from −100 to +100 mV. ***B***, Quantifications showing substantial reductions of whole-cell currents in cells expressing $TRPC5^{DN}$ or $TRPC5^{DN}$/$TRPC5^{WT}$, as compared with $TRPC5^{WT}$, at both −100 and +100 mV ($TRPC5^{WT}$: $n = 16$ cells; $TRPC5^{DN}$: $n = 18$ cells; co-transfection: $n = 15$ cells; one-way ANOVA followed by Tukey's *post hoc* test, $TRPC5^{DN}$ or $TRPC5^{DN}$/$TRPC5^{WT}$ vs $TRPC5^{WT}$: ***$p < 0.001$). ***C***, Normalized increases of synGCaMP6f fluorescence induced by single AP in control or $TRPC5^{DN}$-expressing neurons. Gray lines are mean fluorescence changes of individual ROIs from each coverslip, with black and red line as the averaged response of individual coverslips from control and $TRPC5^{DN}$ groups, respectively. Raw data for Ca^{2+} increases induced by single AP are presented in Figure 9. ***D***, Bar graph comparing peak synGCaMP6f values as shown in ***C*** reveals no change in Ca^{2+} signals in $TRPC5^{DN}$-expressing neurons (control: $n = 20$ coverslips; $TRPC5^{DN}$: $n = 19$ coverslips, $p = 0.4639$). ***E***, Normalized SynGCaMP6f increases induced by 100 APs at 20 Hz in control or $TRPC5^{DN}$-expressing neurons. Gray lines are mean fluorescence changes of individual ROIs from each coverslip, with black or red line as the averaged response of individual coverslips from control or $TRPC5^{DN}$ group. ***F***, Bar graph comparing peak Ca^{2+} values as shown in ***E*** demonstrates a significant decrease of Ca^{2+} signals in $TRPC5^{DN}$-expressing neurons (control: $n = 22$ coverslips; $SphK1^{DN}$: $n = 22$ coverslips). ***G***, Representative whole-cell TRPC5 currents before (black) and after (red) 5 μM S1P application, recorded from a $TRPC5^{WT}$-expressing HEK293 cell, in response to a voltage ramp from −100 to +100 mV. ***H***, Quantifications showing significant increases of whole-cell TRPC5 currents by S1P application (red vs black) at both +100 mV (top) and −100 mV (bottom; $n = 16$ cells; paired t test, ***$p < 0.001$). ***I***, Normalized fluorescence increases of SynGCaMP6f signals induced by 100 APs at 20 Hz from $TRPC5^{DN}$ or $SphK1^{DN}$/$TRPC5^{DN}$-expressing neurons. Gray lines are mean fluorescence changes of individual ROIs from each coverslip, with black or red line as the averaged response of individual coverslips from $TRPC5^{DN}$ or $SphK1^{DN}$/$TRPC5^{DN}$-expressing neurons. ***J***, Bar graph comparing peak Ca^{2+} values as shown in ***I*** demonstrates that $SphK1^{DN}$ had no significant effects on Ca^{2+} signals in $TRPC5^{DN}$-expressing neurons ($TRPC5^{DN}$: $n = 24$ coverslips; $SphK1^{DN}$/$TRPC5^{DN}$: $n = 24$ coverslips, $p = 0.4856$). *$p < 0.05$, unpaired two-tailed Student's t test in ***D***, ***F***, and ***J***.

enhanced by exogenously applied S1P ($p < 0.001$; Fig. 8*G*, *H*), confirming the S1P-mediated regulation of TRPC5 as reported by previous Ca^{2+} imaging studies (Xu et al., 2006; Naylor et al., 2016). Consistent with a previous study on hippocampal neurons using transgenic knock-out (KO) and knock-in mice (Schwarz et al., 2019), $TRPC5^{DN}$ induced a significant decrease in presynaptic Ca^{2+} levels in response to 100 APs at 20-Hz stimulations ($p < 0.05$; Fig. 8*E*,*F*) rather than single AP stimulation ($p > 0.05$; Figs. 8*C*,*D*, 9), implying an importance of TRPC5 in maintaining presynaptic

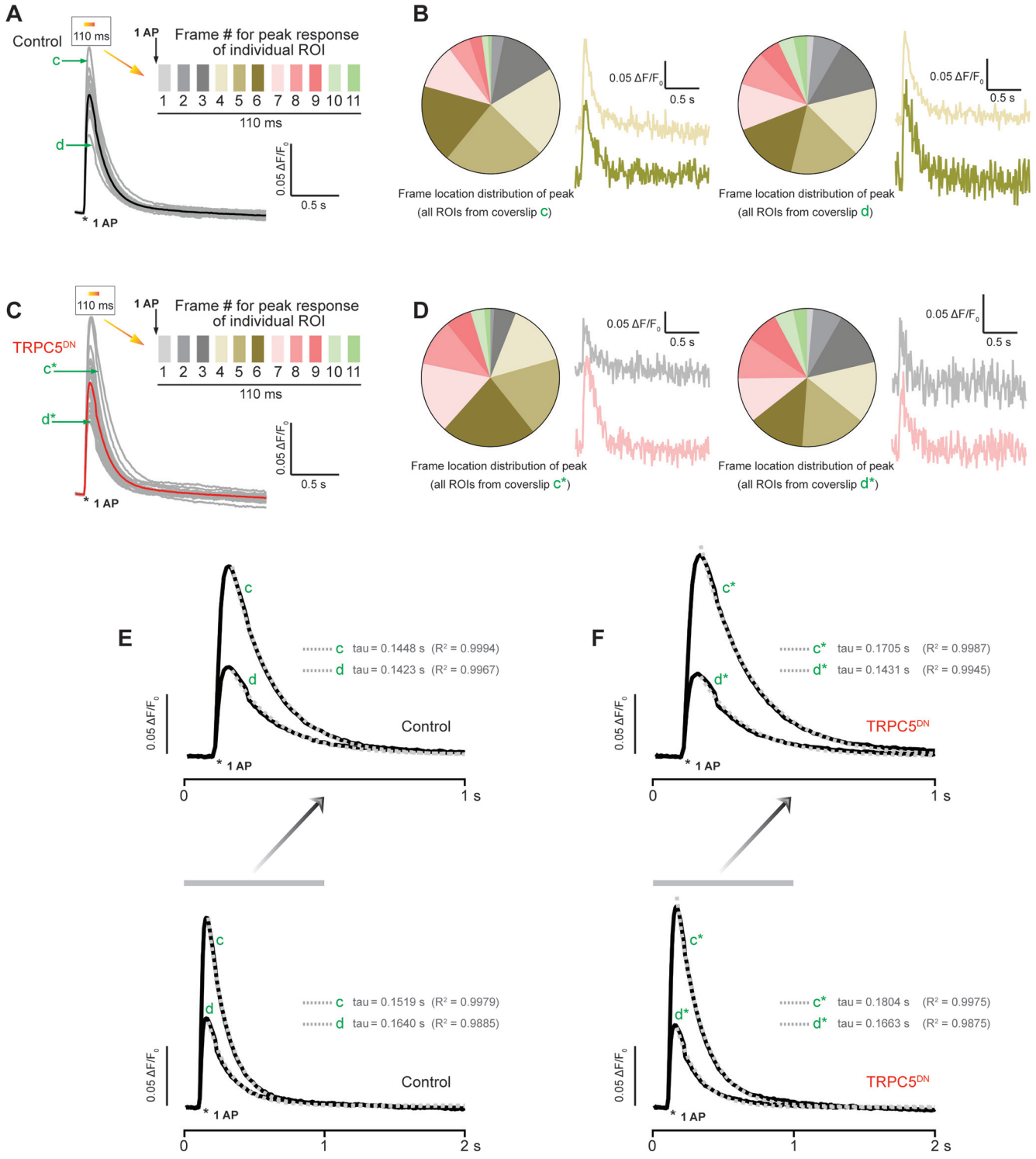

Figure 9. Raw data for Ca^{2+} increases induced by single AP in control and $TRPC5^{DN}$-expressing neurons. ***A***, Time courses of normalized synGCaMP6f increases induced by single AP in control neurons. Gray lines are mean fluorescence changes of individual ROIs from each coverslip, with the black line as the averaged response of individual coverslips. As shown on top of the traces, peak Ca^{2+} signal induced by 1 AP from individual ROIs occurred within 110 ms, ranging from the first to 11^{th} frame after stimulus as shown with color coded diagram (upper right). ***B***, Color coded pie charts showing frame location distributions of Ca^{2+} peaks for all ROIs in coverslips "c" (left) and "d" (right). Along with each pie chart, two color coded traces from each coverslip showed representative ROIs with Ca^{2+} peaked at the fourth and sixth frame. ***C***, Time courses of normalized synGCaMP6f increases induced by single AP in $TRPC5^{DN}$-expressing neurons. Gray lines are mean fluorescence changes of individual ROIs from each coverslip, with the red line as the averaged response of individual coverslips. As shown on top of the traces, peak Ca^{2+} signal induced by 1 AP from individual ROIs occurred within 110 ms, ranging from the first to 11th frame after stimulus as shown with color coded diagram (upper right). ***D***, Color coded pie charts showing frame location distributions of Ca^{2+} peaks from all ROIs in coverslips "c*" (left) and "d*" (right) from $TRPC5^{DN}$ group. Along with each pie chart, two color coded traces from each coverslip showed representative ROIs with Ca^{2+} peaked at the second and seventh frame. ***E***, Truncated (above) and full (below) time courses of mean synGCaMP6f signals induced by single AP of coverslip "c" or "d" from control group, with decay phases of Ca^{2+} signals fitted by single exponential functions (dotted gray lines). ***F***, Truncated (above) and full (below) time courses of mean synGCaMP6f signals induced by single AP of coverslip "c*" or "d*" from $TRPC5^{DN}$ group with decay phases of mean Ca^{2+} signals fitted by single exponential functions (dotted gray lines).

Ca^{2+} levels during prolonged stimulations. Moreover, in contrast to an inhibition of presynaptic Ca^{2+} influx in control neurons (Fig. 5*C*,*D*), $SphK1^{DN}$ had no obvious effects on presynaptic Ca^{2+} levels in response to 100 APs at 20-Hz stimulations in $TRPC5^{DN}$-expressing neurons ($p > 0.05$; Fig. 8*I*,*J*), pointing out that Ca^{2+} influx via TRPC5 channels may be critical for the role of the SphK1/S1P axis in presynaptic Ca^{2+} signaling during prolonged stimulations.

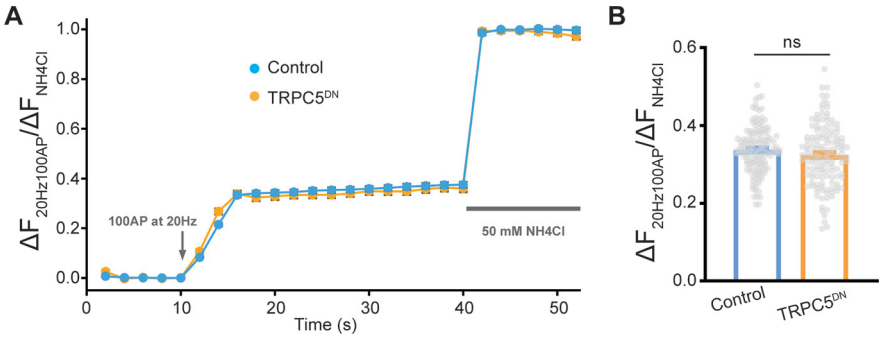

Figure 10. $TRPC5^{DN}$ has no significant effect on synaptic vesicle exocytosis in neurons. ***A***, In the presence of bafilomycin A1, time courses of averaged increases in the sypHy signals induced by 100 APs at 20-Hz stimulations in control or $TRPC5^{DN}$-expressing neurons. Fluorescence increases induced by electrical stimulations are normalized to that by NH_4Cl to minimize potential impacts from sypHy expression variations. ***B***, Bar graph showing comparable peak values of normalized fluorescence increases in control or $TRPC5^{DN}$-expressing neurons (control: $n = 143$ boutons; $TRPC5^{DN}$: $n = 139$ boutons; $p = 0.1096$). Unpaired two-tailed Student's *t* test. ns: not statistically significant.

TRPC5 is critical for the role of the SphK1/S1P axis in synaptic vesicle endocytosis

Consistent with critical roles of TRPC5 channels in mediating Ca^{2+} influx on train stimulations (Fig. 8*E*,*F*), $TRPC5^{DN}$ induced a significant increase in the time constant of sypHy signal decay ($p < 0.05$; Fig. 11*A*,*B*), implying an importance of Ca^{2+} influx via TRPC5 in synaptic vesicle endocytosis. On the other hand, there was no change in sypHy fluorescence increase induced by electric stimulations in $TRPC5^{DN}$-expressing neurons as compared with control neurons ($p > 0.05$; Fig. 11*C*,*D*). We reasoned that any potential reductions in sypHy increase induced by $TRPC5^{DN}$ could be masked by a comparable reduction in endocytosis during stimulation, since a significant defect in synaptic vesicle endocytosis induced by $TRPC5^{DN}$ has been observed as shown in Figure 11*A*,*B*. Indeed, in the presence of bafilomycin to block vesicle reacidification because of endocytosis, $TRPC5^{DN}$ induced a small, although nonsignificant, reduction in the increase of pHluorin signals induced by 100 APs at 20-Hz stimulations ($p > 0.05$; Fig. 10). Collectively, our data indicate that Ca^{2+} influx via TRPC5 may be specifically required for synaptic vesicle endocytosis. Given the dependence on Ca^{2+} influx via TRPC5 for the role of the SphK1/S1P axis in presynaptic Ca^{2+} levels (Fig. 8*I*,*J*), we then analyzed effects of $SphK1^{DN}$ on synaptic vesicle endocytosis in $TRPC5^{DN}$-expressing neurons. In contrast to an increase in the time constant of sypHy signal decay after the cessation of stimulations induced by $SphK1^{DN}$ expression in control neurons (Fig. 2*A*,*B*), $SphK1^{DN}$ induced no detectable changes in this parameter in $TRPC5^{DN}$-expressing neurons (Fig. 11*E*,*F*), indicating that Ca^{2+} via TRPC5 channels may be necessary for the SphK1/S1P axis-mediated action in synaptic vesicle endocytosis. However, similar as $SphK1^{DN}$ expression in control neurons (Fig. 1*C*,*D*), $SphK1^{DN}$ reduced the increase in pHluorin signals induced by 100 APs at 20 Hz in $TRPC5^{DN}$-expressing neurons ($p < 0.001$; Fig. 11*G*,*H*), indicating that the role of the SphK1/S1P axis in exocytosis may be independent of TRPC5. Taken together, our data point out that the regulation of TRPC5 channels by the SphK1/S1P axis may be especially crucial for synaptic vesicle endocytosis in neurons.

Discussion

By showing an endocytic defect induced by $SphK1^{DN}$ (Fig. 2), we demonstrate an essential role of the SphK1/S1P axis in synaptic vesicle endocytosis in neurons. This conclusion is reiterated by the evidence that the $SphK1^{DN}$ induced endocytic defect can be rescued by a clinical S1P analog FTY720 (Fig. 4*C*,*D*). Meanwhile, Ca^{2+} imaging shows that $SphK1^{DN}$ induces a decreased Ca^{2+} level during prolonged stimulations in control neurons (Fig. 5), indicating an importance of the SphK1/S1P axis in synaptic vesicle endocytosis by regulating presynaptic Ca^{2+} signaling. Furthermore, $SphK1^{DN}$ induced no detectable effects on either presynaptic Ca^{2+} influx or synaptic vesicle endocytosis in $TRPC5^{DN}$-expressing neurons, implying that Ca^{2+} influx via TRPC5 may be necessary for the SphK1/S1P axis-mediated action. Collectively, our data point out that regulations of Ca^{2+} influx via TRPC5 channels by the SphK1/S1P axis may be important for synaptic vesicle endocytosis in neurons. On the other hand, $SphK1^{DN}$ induces a defect in synaptic vesicle exocytosis (Fig. 1), which can also be rescued by exogenous FTY720 application (Fig. 4*A*,*B*), confirming critical roles of the SphK1/S1P axis in synaptic vesicle exocytosis as reported (Kajimoto et al., 2007; Chan et al., 2012; Riganti et al., 2016; Z. J. Jiang et al., 2019b). Moreover, this FTY720-mediated rescue is abolished by S1P receptor inhibitors (Fig. 4*A*,*B*), suggesting that S1P receptors may be responsible for the action of the SphK1/S1P axis in synaptic vesicle exocytosis in neurons. In view of different downstream molecular pathways identified in our study, the SphK1/S1P axis is inferred to regulate synaptic vesicle exocytosis and endocytosis through distinct mechanisms.

The SphK1/S1P axis regulates RRP during exocytosis

Our data showed that synaptic vesicle exocytosis induced by 100 APs at 20-Hz stimulations is reduced by $SphK1^{DN}$ (Fig. 1*C*–*F*), indicating a role of the SphK1/S1P axis in synaptic vesicle exocytosis. This conclusion agrees with previous studies in neurons from *C. elegans* (Chan et al., 2012), mouse neuroendocrine cells (Pan et al., 2006; Z.C. Jiang et al., 2019a) and hippocampal neurons (Kajimoto et al., 2007; Kanno et al., 2010; Riganti et al., 2016), frog neuromuscular junctions (Brailoiu et al., 2002), and zona glomerulosa cells (Brizuela et al., 2007). It is acknowledged that two vesicle pools, TRP and RRP, are essential in determining the amount of exocytosis on stimulations (S.H. Kim and Ryan, 2010; Alabi and Tsien, 2012; Baumgart et al., 2015). Our imaging data reveal that $SphK1^{DN}$ reduces RRP size and slows down RRP replenishment (Fig. 1*J*–*M*) with no obvious effects on TRP size or its depletion kinetics (Fig. 1*G*–*I*), indicating a physiological role of the SphK1/S1P axis in regulating the size and replenishment of RRP during exocytosis. Consistently, a previous study implies that exogenous S1P addition may increase the size of

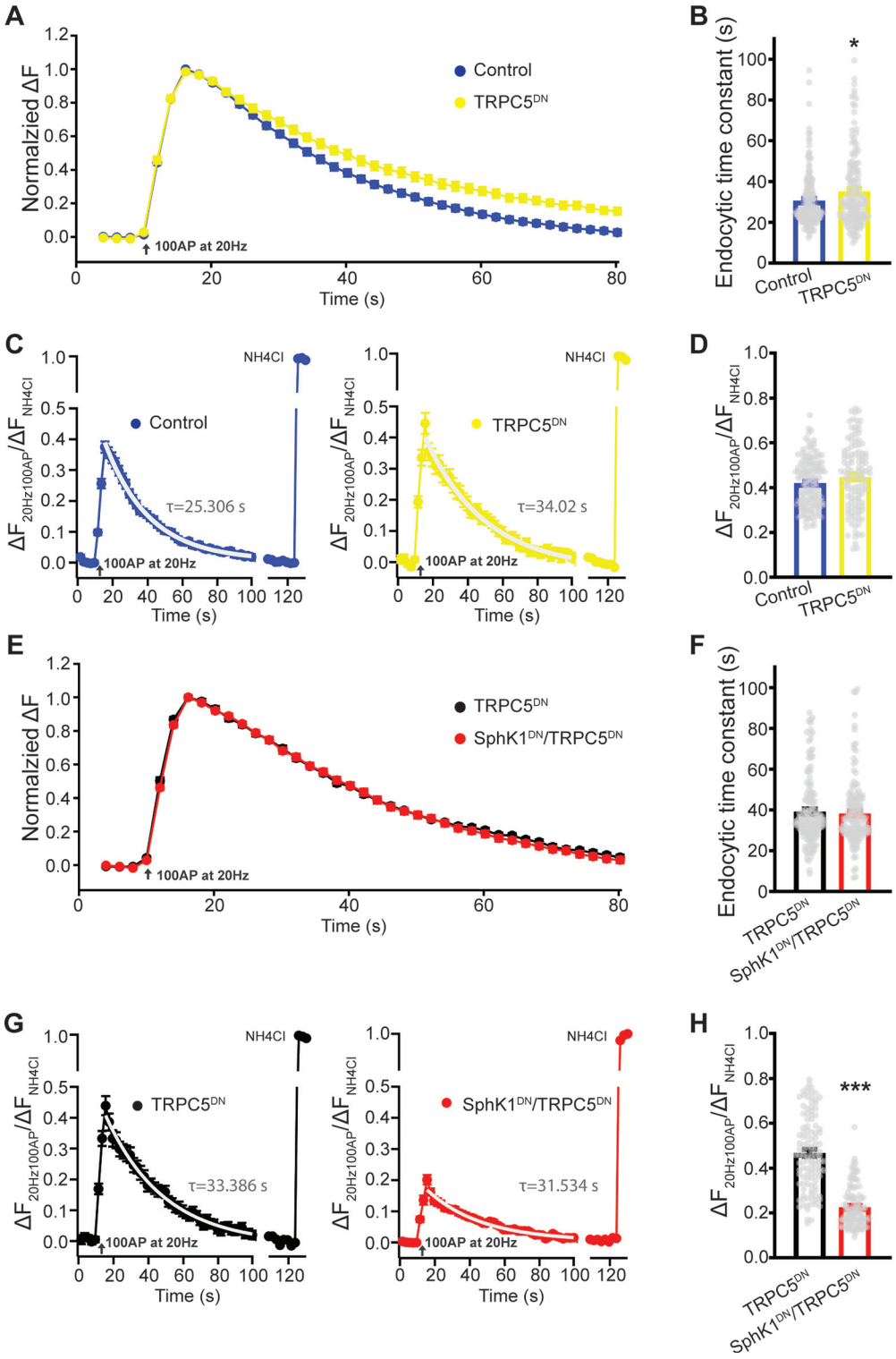

Figure 11. TRPC5 is required for the role of the SphK1/S1P axis in synaptic vesicle endocytosis in neurons. ***A***, Normalized changes of sypHy signals in response to 100 APs at 20-Hz stimulations in control and TRPC5^{DN}-expressing neurons. ***B***, Bar graph showing an increase in the endocytic time constant in TRPC5^{DN}-expressing neurons (control: $n = 163$ boutons; TPRC5^{DN}: $n = 154$ boutons). ***C***, Time courses of averaged increases in the sypHy signals induced by 100 APs at 20-Hz stimulations in control or TRPC5^{DN}-expressing neurons. Fluorescence increases induced by electrical stimulations are normalized to that by NH_4Cl perfusion at the end of each trial to minimize potential impacts of sypHy expression variations. The time constant (τ) of pHluorin signal decay for the averaged response of control or TRPC5^{DN} group was obtained by fitting the fluorescence decay with a single exponential function (gray lines). ***D***, Bar graph showing comparable peak values of normalized fluorescence increases in control or TRPC5^{DN}-expressing neurons (control: $n = 142$ boutons; TRPC5DN: $n = 118$ boutons; $p = 0.1002$). In the presence of bafilomycin, TRRPC5^{DN} induces a small, but nonsignificant, reduction in exocytosis (Fig. 10). ***E***, Normalized changes of sypHy fluorescence in TRPC5^{DN} or SphK1^{DN}/TRPC5^{DN}-expressing neurons. ***F***, Bar graph showing that SphK1^{DN} had no detectable effects on the endocytic time constant in TRPC5^{DN}-expressing neurons (TPRC5^{DN}: $n = 150$ boutons; SphK1^{DN}/TRPC5^{DN}: $n = 150$ boutons, $p = 0.6463$). ***G***, Time courses of averaged increases in the sypHy signals induced by a 100 APs at 20-Hz stimulation in TRPC5^{DN} or SphK1^{DN}/TRPC5^{DN}-expressing neurons. Fluorescence increases induced by electrical stimulations are normalized to that by NH_4Cl perfusion at the end of each trial. The time constant (τ) of pHluorin signal decay for the averaged response of TRPC5^{DN} or SphK1^{DN}/TRPC5^{DN} group was obtained by fitting the fluorescence decay with a single exponential function (gray lines). ***H***, Bar graph showing that SphK1^{DN} causes a significant reduction of exocytosis in TRPC5^{DN}-expressing neurons (TRPC5^{DN}: $n = 115$ boutons; SphK1^{DN}/TRPC5^{DN}: $n = 113$ boutons). *$p < 0.05$, ***$p < 0.001$, unpaired two-tailed Student's t test.

RRP, measured as sucrose evoked EPSCs (Riganti et al., 2016). The RRP regulation by the SphK1/S1P axis may reflect its function in vesicle docking and priming, since FTY720 has been implied to affect docking/priming process in primary rat cultured astrocytes, a non-neuronal cell (Trkov et al., 2012). Alternatively, the SphK1/S1P may control RRP by modulating localization of synapsin I (Riganti et al., 2016), a major synaptic vesicle associated phosphoprotein regulating RRP size (Baldelli et al., 2007).

The SphK1/S1P axis promotes vesicle endocytosis in neuronal cells

By showing that $SphK1^{DN}$ slowed down sypHy fluorescence decay after the cessation of stimulations at both room and physiological temperatures (Fig. 2), our data provide the first evidence for critical roles of the SphK1/S1P axis in synaptic vesicle endocytosis in neurons. Additionally, single vesicle endocytosis monitored using cell-attached capacitance recordings in chromaffin cells reveals an importance of the SphK1/S1P axis in vesicle fission during endocytosis (Fig. 3). Our findings thus expand the reported roles of the SphK1/S1P axis in endocytic trafficking in non-neuronal cells (Yonamine et al., 2011; Shen et al., 2014; Young et al., 2016; Lima et al., 2017) to neuronal endocytosis. Based on the documented importance of endocytosis for the synaptic vesicle reavailability in RRP (Pyle et al., 2000; Granseth and Lagnado, 2008; Cheung et al., 2010; Rizzoli, 2014; Kyung et al., 2018; Y. Kim et al., 2020), the role of the SphK1/S1P axis in synaptic vesicle endocytosis may account for the $SphK1^{DN}$-induced disruption in RRP replenishment we have observed (Fig. 1*L*,*M*).

The regulation of TRPC5 by the SphK1/S1P axis is critical for synaptic vesicle endocytosis

$TRPC5^{DN}$ reduced Ca^{2+} increase induced by 100 APs at 20 Hz (Fig. 8*E*,*F*) rather than single AP (Fig. 8*C*,*D*), suggesting critical roles of TRPC5 in presynaptic Ca^{2+} signaling during prolonged stimulations. Our results are in line with a previous study using transgenic KO and knock-in mice, demonstrating an importance of TRPC5 channels, independent of VGCCs, in presynaptic Ca^{2+} influx during stimulation trains (Schwarz et al., 2019). Furthermore, $TRPC5^{DN}$ slowed down sypHy signal decay after stimulations (Fig. 11*A*,*B*), indicating that Ca^{2+} influx via TRPC5 channels may be critical for synaptic vesicle endocytosis in neurons. It is of note that previous studies have identified that Ca^{2+} influx via TRPM7 (Z.J. Jiang et al., 2021), another TRP superfamily member (Clapham, 2003), and Flower (C.K. Yao et al., 2017), a Ca^{2+} permeable protein with Ca^{2+} selectivity filter similar as TRPV5 and TRPV6 (C.K. Yao et al., 2009), may be crucial for synaptic vesicle endocytosis in mammalian neurons. Along this line, it would be interesting to find out the importance of other members of TRP superfamily, which are Ca^{2+} permeable and widely expressed in the brain (Ramsey et al., 2006; Venkatachalam and Montell, 2007; Sawamura et al., 2017; Koivisto et al., 2022), in synaptic vesicle endocytosis in the mammalian brain. On the other hand, Ca^{2+} influx via TRPC5 has been previously shown to be important for short-term plasticity of fast glutamatergic synapses (Schwarz et al., 2019). Given the well-established significance of synaptic vesicle endocytosis in short-term synaptic plasticity (Zucker and Regehr, 2002; Granseth and Lagnado, 2008; Hosoi et al., 2009; Regehr, 2012; Y. Hua et al., 2013; Z.J. Jiang et al., 2021), our discovery suggests that the previously reported functions of TRPC5 in short-term plasticity may reflect its role in synaptic vesicle endocytosis in neurons.

The present study using electrophysiological recordings and previous Ca^{2+} imaging assays in HEK293 cells have testified the role of S1P as a physiological activator for TRPC5 channels (Xu et al., 2006; Naylor et al., 2016). Our Ca^{2+} imaging studies in neurons shows that $SphK1^{DN}$ induces a reduction in presynaptic synGCaMP6f signal increase in response to 100 APs at 20-Hz stimulations in control (Fig. 5*C*,*D*) but not $TRPC5^{DN}$-expressing neurons (Fig. 8*I*,*J*), indicating that the SphK1/S1P axis may be crucial for presynaptic Ca^{2+} signaling via regulating TRPC5 channels during prolonged stimulations. This finding is likely to provide novel mechanistic insights into the role of S1P, an enigmatic signaling molecule, in Ca^{2+} homeostasis in the mammalian brain (Spiegel and Milstien, 2003; Karunakaran and van Echten-Deckert, 2017). In parallel, $SphK1^{DN}$ slows down sypHy fluorescence decay after the cessation of stimulations in control (Fig. 2*A*,*B*) but not $TRPC5^{DN}$-expressing neurons (Fig. 11*E*,*F*), indicating an importance of TRPC5 in the SphK1/S1P axis-mediated regulation of synaptic vesicle endocytosis. Collectively, our data point out regulations of Ca^{2+} influx via TRPC5 by the SphK1/S1P axis may be critical for synaptic vesicle endocytosis. This discovery may thus provide novel mechanistic implications for parallel involvements of TRPC5 and S1P in brain functions under physiological and pathologic conditions and pain-related behaviors in mice and human (Camprubí-Robles et al., 2013; Hong et al., 2015, 2020; Weth-Malsch et al., 2016; Bröker-Lai et al., 2017; Di Pardo et al., 2017; Karunakaran and van Echten-Deckert, 2017; Hill et al., 2018; Sadler et al., 2021).

Implications to neurologic disorders

The SphK1/S1P axis and synaptic vesicle endocytosis have been linked to the same group of neurologic disorders, including Parkinson's disease (Pyszko and Strosznajder, 2014), Huntington's disease (Di Pardo et al., 2019), Alzheimer's disease (Ceccom et al., 2014; Couttas et al., 2014), and multiple sclerosis (Subei and Cohen, 2015; Mao-Draayer et al., 2017). By identifying for the first time a role of the SphK1/S1P axis in synaptic vesicle endocytosis, our study indicates that impaired regulations of the SphK1/S1P axis in synaptic vesicle endocytosis may contribute to pathophysiological mechanisms of these neurologic disorders (Couttas et al., 2014; Pirhaji et al., 2016; Schreij et al., 2016; Lee et al., 2018; Di Pardo et al., 2019; McAdam et al., 2020; Pensalfini et al., 2020). Meanwhile, it is worth mentioning that the SphK1/S1P axis has recently been identified as a key regulator for autophagy in neurons (Moruno Manchon et al., 2015, 2016), and dysfunction of autophagy is identified in many neurologic diseases (Menzies et al., 2017; Malik et al., 2019; Klionsky et al., 2021). Indeed, there is an interdependency of autophagy and synaptic vesicle endocytosis within presynaptic terminals (Limanaqi et al., 2018; Overhoff et al., 2021; Yang et al., 2022). As the SphK1/S1P axis may modulate the coordination between autophagy and endocytic membrane trafficking in mouse embryonic fibroblasts (Young et al., 2016), it would be interesting to understand whether the SphK1/S1P axis may regulate the interplay between autophagy and synaptic vesicle endocytosis within presynaptic terminals in the future.

References

Alabi AA, Tsien RW (2012) Synaptic vesicle pools and dynamics. Cold Spring Harb Perspect Biol 4:a013680.

Alemany R, van Koppen CJ, Danneberg K, Ter Braak M, Meyer Zu Heringdorf D (2007) Regulation and functional roles of sphingosine kinases. Naunyn Schmiedebergs Arch Pharmacol 374:413–428.

Ali R, Nicholas RS, Muraro PA (2013) Drugs in development for relapsing multiple sclerosis. Drugs 73:625–650.

Alsaqati M, Thomas RS, Kidd EJ (2018) Proteins involved in endocytosis are upregulated by ageing in the normal human brain: implications for the development of Alzheimer's disease. J Gerontol A Biol Sci Med Sci 73:289–298.

Ammar MR, Kassas N, Chasserot-Golaz S, Bader MF, Vitale N (2013) Lipids in regulated exocytosis: what are they doing? Front Endocrinol (Lausanne) 4:125.

Balaji J, Ryan TA (2007) Single-vesicle imaging reveals that synaptic vesicle exocytosis and endocytosis are coupled by a single stochastic mode. Proc Natl Acad Sci U S A 104:20576–20581.

Baldelli P, Fassio A, Valtorta F, Benfenati F (2007) Lack of synapsin I reduces the readily releasable pool of synaptic vesicles at central inhibitory synapses. J Neurosci 27:13520–13531.

Barron JC, Hurley EP, Parsons MP (2021) Huntingtin and the Synapse. Front Cell Neurosci 15:689332.

Bassani S, Cingolani LA, Valnegri P, Folci A, Zapata J, Gianfelice A, Sala C, Goda Y, Passafaro M (2012) The X-linked intellectual disability protein TSPAN7 regulates excitatory synapse development and AMPAR trafficking. Neuron 73:1143–1158.

Baumgart JP, Zhou ZY, Hara M, Cook DC, Hoppa MB, Ryan TA, Hemmings HC Jr (2015) Isoflurane inhibits synaptic vesicle exocytosis through reduced Ca2+ influx, not Ca2+-exocytosis coupling. Proc Natl Acad Sci U S A 112:11959–11964.

Blair NT, Kaczmarek JS, Clapham DE (2009) Intracellular calcium strongly potentiates agonist-activated TRPC5 channels. J Gen Physiol 133:525–546.

Bolte S, Cordelières FP (2006) A guided tour into subcellular colocalization analysis in light microscopy. J Microsc 224:213–232.

Bonhoure E, Pchejetski D, Aouali N, Morjani H, Levade T, Kohama T, Cuvillier O (2006) Overcoming MDR-associated chemoresistance in HL-60 acute myeloid leukemia cells by targeting sphingosine kinase-1. Leukemia 20:95–102.

Brailoiu E, Cooper RL, Dun NJ (2002) Sphingosine 1-phosphate enhances spontaneous transmitter release at the frog neuromuscular junction. Br J Pharmacol 136:1093–1097.

Brizuela L, Rábano M, Gangoiti P, Narbona N, Macarulla JM, Trueba M, Gómez-Muñoz A (2007) Sphingosine-1-phosphate stimulates aldosterone secretion through a mechanism involving the PI3K/PKB and MEK/ERK 1/2 pathways. J Lipid Res 48:2264–2274.

Brockhaus J, Brüggen B, Missler M (2019) Imaging and analysis of presynaptic calcium influx in cultured neurons using synGCaMP6f. Front Synaptic Neurosci 11:12.

Bröker-Lai J, Kollewe A, Schindeldecker B, Pohle J, Nguyen Chi V, Mathar I, Guzman R, Schwarz Y, Lai A, Weißgerber P, Schwegler H, Dietrich A, Both M, Sprengel R, Draguhn A, Köhr G, Fakler B, Flockerzi V, Bruns D, Freichel M (2017) Heteromeric channels formed by TRPC1, TRPC4 and TRPC5 define hippocampal synaptic transmission and working memory. EMBO J 36:2770–2789.

Bryan L, Kordula T, Spiegel S, Milstien S (2008) Regulation and functions of sphingosine kinases in the brain. Biochim Biophys Acta 1781:459–466.

Camprubí-Robles M, Mair N, Andratsch M, Benetti C, Beroukas D, Rukwied R, Langeslag M, Proia RL, Schmelz M, Ferrer Montiel AV, Haberberger RV, Kress M (2013) Sphingosine-1-phosphate-induced nociceptor excitation and ongoing pain behavior in mice and humans is largely mediated by S1P3 receptor. J Neurosci 33:2582–2592.

Cataldo AM, Peterhoff CM, Troncoso JC, Gomez-Isla T, Hyman BT, Nixon RA (2000) Endocytic pathway abnormalities precede amyloid beta deposition in sporadic Alzheimer's disease and Down syndrome: differential effects of APOE genotype and presenilin mutations. Am J Pathol 157:277–286.

Ceccom J, Loukh N, Lauwers-Cances V, Touriol C, Nicaise Y, Gentil C, Uro-Coste E, Pitson S, Maurage CA, Duyckaerts C, Cuvillier O, Delisle MB (2014) Reduced sphingosine kinase-1 and enhanced sphingosine 1-phosphate lyase expression demonstrate deregulated sphingosine 1-phosphate signaling in Alzheimer's disease. Acta Neuropathol Commun 2:12.

Chan JP, Hu Z, Sieburth D (2012) Recruitment of sphingosine kinase to presynaptic terminals by a conserved muscarinic signaling pathway promotes neurotransmitter release. Genes Dev 26:1070–1085.

Chanaday NL, Cousin MA, Milosevic I, Watanabe S, Morgan JR (2019) The synaptic vesicle cycle revisited: new insights into the modes and mechanisms. J Neurosci 39:8209–8216.

Chen TW, Wardill TJ, Sun Y, Pulver SR, Renninger SL, Baohan A, Schreiter ER, Kerr RA, Orger MB, Jayaraman V, Looger LL, Svoboda K, Kim DS (2013) Ultrasensitive fluorescent proteins for imaging neuronal activity. Nature 499:295–300.

Cheung G, Jupp OJ, Cousin MA (2010) Activity-dependent bulk endocytosis and clathrin-dependent endocytosis replenish specific synaptic vesicle pools in central nerve terminals. J Neurosci 30:8151–8161.

Chiba K, Adachi K (2012) Sphingosine 1-phosphate receptor 1 as a useful target for treatment of multiple sclerosis. Pharmaceuticals (Basel) 5:514–528.

Clapham DE (2003) TRP channels as cellular sensors. Nature 426:517–524.

Cousin MA (2000) Synaptic vesicle endocytosis: calcium works overtime in the nerve terminal. Mol Neurobiol 22:115–128.

Couttas TA, Kain N, Daniels B, Lim XY, Shepherd C, Kril J, Pickford R, Li H, Garner B, Don AS (2014) Loss of the neuroprotective factor Sphingosine 1-phosphate early in Alzheimer's disease pathogenesis. Acta Neuropathol Commun 2:9.

Davare MA, Fortin DA, Saneyoshi T, Nygaard S, Kaech S, Banker G, Soderling TR, Wayman GA (2009) Transient receptor potential canonical 5 channels activate Ca2+/calmodulin kinase Igamma to promote axon formation in hippocampal neurons. J Neurosci 29:9794–9808.

de Juan-Sanz J, Holt GT, Schreiter ER, de Juan F, Kim DS, Ryan TA (2017) Axonal endoplasmic reticulum Ca(2+) content controls release probability in CNS nerve terminals. Neuron 93:867–881.e6.

Dernick G, Gong LW, Tabares L, Alvarez de Toledo G, Lindau M (2005) Patch amperometry: high-resolution measurements of single-vesicle fusion and release. Nat Methods 2:699–708.

Di Menna L, Molinaro G, Di Nuzzo L, Riozzi B, Zappulla C, Pozzilli C, Turrini R, Caraci F, Copani A, Battaglia G, Nicoletti F, Bruno V (2013) Fingolimod protects cultured cortical neurons against excitotoxic death. Pharmacol Res 67:1–9.

Di Pardo A, Maglione V (2018) Sphingolipid metabolism: a new therapeutic opportunity for brain degenerative disorders. Front Neurosci 12:249.

Di Pardo A, Amico E, Basit A, Armirotti A, Joshi P, Neely MD, Vuono R, Castaldo S, Digilio AF, Scalabrì F, Pepe G, Elifani F, Madonna M, Jeong SK, Park BM, D'Esposito M, Bowman AB, Barker RA, Maglione V (2017) Defective Sphingosine-1-phosphate metabolism is a druggable target in Huntington's disease. Sci Rep 7:5280.

Di Pardo A, Pepe G, Castaldo S, Marracino F, Capocci L, Amico E, Madonna M, Giova S, Jeong SK, Park BM, Park BD, Maglione V (2019) Stimulation of sphingosine kinase 1 (SPHK1) is beneficial in a Huntington's disease pre-clinical model. Front Mol Neurosci 12:100.

Edsall LC, Spiegel S (1999) Enzymatic measurement of sphingosine 1-phosphate. Anal Biochem 272:80–86.

Fernández-Alfonso T, Ryan TA (2004) The kinetics of synaptic vesicle pool depletion at CNS synaptic terminals. Neuron 41:943–953.

Fukuda Y, Kihara A, Igarashi Y (2003) Distribution of sphingosine kinase activity in mouse tissues: contribution of SPHK1. Biochem Biophys Res Commun 309:155–160.

Ghasemi R, Dargahi L, Ahmadiani A (2016) Integrated sphingosine-1 phosphate signaling in the central nervous system: from physiological equilibrium to pathological damage. Pharmacol Res 104:156–164.

Ghosh TK, Bian J, Gill DL (1990) Intracellular calcium release mediated by sphingosine derivatives generated in cells. Science 248:1653–1656.

Gomez-Brouchet A, Pchejetski D, Brizuela L, Garcia V, Altié MF, Maddelein ML, Delisle MB, Cuvillier O (2007) Critical role for sphingosine kinase-1 in regulating survival of neuroblastoma cells exposed to amyloid-beta peptide. Mol Pharmacol 72:341–349.

Gomis A, Soriano S, Belmonte C, Viana F (2008) Hypoosmotic- and pressure-induced membrane stretch activate TRPC5 channels. J Physiol 586:5633–5649.

Gong LW, Di Paolo G, Diaz E, Cestra G, Diaz ME, Lindau M, De Camilli P, Toomre D (2005) Phosphatidylinositol phosphate kinase type I gamma regulates dynamics of large dense-core vesicle fusion. Proc Natl Acad Sci U S A 102:5204–5209.

Granseth B, Lagnado L (2008) The role of endocytosis in regulating the strength of hippocampal synapses. J Physiol 586:5969–5982.

Granseth B, Odermatt B, Royle SJ, Lagnado L (2006) Clathrin-mediated endocytosis is the dominant mechanism of vesicle retrieval at hippocampal synapses. Neuron 51:773–786.

Greka A, Navarro B, Oancea E, Duggan A, Clapham DE (2003) TRPC5 is a regulator of hippocampal neurite length and growth cone morphology. Nat Neurosci 6:837–845.

Griggs RB, Nguyen DVM, Yermakov LM, Jaber JM, Shelby JN, Steinbrunner JK, Miller JA, Gonzalez-Islas C, Wenner P, Susuki K (2021) The type 2 diabetes factor methylglyoxal mediates axon initial segment shortening and alters neuronal function at the cellular and network levels. eNeuro 8: ENEURO.0201-21.2021.

Haucke V, Neher E, Sigrist SJ (2011) Protein scaffolds in the coupling of synaptic exocytosis and endocytosis. Nat Rev Neurosci 12:127–138.

Helbig I, et al. (2019) A recurrent missense variant in AP2M1 impairs Clathrin-mediated endocytosis and causes developmental and epileptic encephalopathy. Am J Hum Genet 104:1060–1072.

Hill RZ, Hoffman BU, Morita T, Campos SM, Lumpkin EA, Brem RB, Bautista DM (2018) The signaling lipid sphingosine 1-phosphate regulates mechanical pain. Elife 7:e33285.

Hong C, Seo H, Kwak M, Jeon J, Jang J, Jeong EM, Myeong J, Hwang YJ, Ha K, Kang MJ, Lee KP, Yi EC, Kim IG, Jeon JH, Ryu H, So I (2015) Increased TRPC5 glutathionylation contributes to striatal neuron loss in Huntington's disease. Brain 138:3030–3047.

Hong C, Jeong B, Park HJ, Chung JY, Lee JE, Kim J, Shin YC, So I (2020) TRP channels as emerging therapeutic targets for neurodegenerative diseases. Front Physiol 11:238.

Hosoi N, Holt M, Sakaba T (2009) Calcium dependence of exo- and endocytotic coupling at a glutamatergic synapse. Neuron 63:216–229.

Hua Y, Woehler A, Kahms M, Haucke V, Neher E, Klingauf J (2013) Blocking endocytosis enhances short-term synaptic depression under conditions of normal availability of vesicles. Neuron 80:343–349.

Hua Z, Leal-Ortiz S, Foss SM, Waites CL, Garner CC, Voglmaier SM, Edwards RH (2011) v-SNARE composition distinguishes synaptic vesicle pools. Neuron 71:474–487.

Itagaki K, Hauser CJ (2003) Sphingosine 1-phosphate, a diffusible calcium influx factor mediating store-operated calcium entry. J Biol Chem 278:27540–27547.

Jiang ZC, Chen XJ, Zhou Q, Gong XH, Chen X, Wu WJ (2019a) Downregulated LRRK2 gene expression inhibits proliferation and migration while promoting the apoptosis of thyroid cancer cells by inhibiting activation of the JNK signaling pathway. Int J Oncol 55:21–34.

Jiang ZJ, Delaney TL, Zanin MP, Haberberger RV, Pitson SM, Huang J, Alford S, Cologna SM, Keating DJ, Gong LW (2019b) Extracellular and intracellular sphingosine-1-phosphate distinctly regulates exocytosis in chromaffin cells. J Neurochem 149:729–746.

Jiang ZJ, Li W, Yao LH, Saed B, Rao Y, Grewe BS, McGinley A, Varga K, Alford S, Hu YS, Gong LW (2021) TRPM7 is critical for short-term synaptic depression by regulating synaptic vesicle endocytosis. Elife 10: e66709.

Kajimoto T, Okada T, Yu H, Goparaju SK, Jahangeer S, Nakamura S (2007) Involvement of sphingosine-1-phosphate in glutamate secretion in hippocampal neurons. Mol Cell Biol 27:3429–3440.

Kaksonen M, Roux A (2018) Mechanisms of clathrin-mediated endocytosis. Nat Rev Mol Cell Biol 19:313–326.

Kanno T, Nishizaki T (2011) Endogenous sphingosine 1-phosphate regulates spontaneous glutamate release from mossy fiber terminals via S1P(3) receptors. Life Sci 89:137–140.

Kanno T, Nishizaki T, Proia RL, Kajimoto T, Jahangeer S, Okada T, Nakamura S (2010) Regulation of synaptic strength by sphingosine 1-phosphate in the hippocampus. Neuroscience 171:973–980.

Karunakaran I, van Echten-Deckert G (2017) Sphingosine 1-phosphate - a double edged sword in the brain. Biochim Biophys Acta Biomembr 1859:1573–1582.

Kempf A, Tews B, Arzt ME, Weinmann O, Obermair FJ, Pernet V, Zagrebelsky M, Delekate A, Iobbi C, Zemmar A, Ristic Z, Gullo M, Spies P, Dodd D, Gygax D, Korte M, Schwab ME (2014) The sphingolipid receptor S1PR2 is a receptor for Nogo-a repressing synaptic plasticity. PLoS Biol 12:e1001763.

Kesharwani A, Schwarz K, Dembla E, Dembla M, Schmitz F (2021) Early changes in Exo- and endocytosis in the EAE mouse model of multiple sclerosis correlate with decreased synaptic ribbon size and reduced ribbon-associated vesicle pools in rod photoreceptor synapses. Int J Mol Sci 22:10789.

Kim SH, Ryan TA (2010) CDK5 serves as a major control point in neurotransmitter release. Neuron 67:797–809.

Kim SH, Ryan TA (2013) Balance of calcineurin Aα and CDK5 activities sets release probability at nerve terminals. J Neurosci 33:8937–8950.

Kim Y, Lee U, Choi C, Chang S (2020) Release mode dynamically regulates the RRP refilling mechanism at individual hippocampal synapses. J Neurosci 40:8426–8437.

Klionsky DJ, et al. (2021) Autophagy in major human diseases. EMBO J 40: e108863.

Koide Y, Hasegawa T, Takahashi A, Endo A, Mochizuki N, Nakagawa M, Nishida A (2002) Development of novel EDG3 antagonists using a 3D database search and their structure-activity relationships. J Med Chem 45:4629–4638.

Koivisto AP, Belvisi MG, Gaudet R, Szallasi A (2022) Advances in TRP channel drug discovery: from target validation to clinical studies. Nat Rev Drug Discov 21:41–59.

Kononenko NL, Haucke V (2015) Molecular mechanisms of presynaptic membrane retrieval and synaptic vesicle reformation. Neuron 85:484–496.

Kyung JW, Cho IH, Lee S, Song WK, Ryan TA, Hoppa MB, Kim SH (2017) Adaptor protein 2 (AP-2) complex is essential for functional axogenesis in hippocampal neurons. Sci Rep 7:41620.

Kyung JW, Kim JM, Lee W, Ha TY, Cha SH, Chung KH, Choi DJ, Jou I, Song WK, Joe EH, Kim SH, Park SM (2018) DJ-1 deficiency impairs synaptic vesicle endocytosis and reavailability at nerve terminals. Proc Natl Acad Sci U S A 115:1629–1634.

Lan T, Liu W, Xie X, Xu S, Huang K, Peng J, Shen X, Liu P, Wang L, Xia P, Huang H (2011) Sphingosine kinase-1 pathway mediates high glucose-induced fibronectin expression in glomerular mesangial cells. Mol Endocrinol 25:2094–2105.

Lee JY, Han SH, Park MH, Baek B, Song IS, Choi MK, Takuwa Y, Ryu H, Kim SH, He X, Schuchman EH, Bae JS, Jin HK (2018) Neuronal SphK1 acetylates COX2 and contributes to pathogenesis in a model of Alzheimer's disease. Nat Commun 9:1479.

Li Z, Burrone J, Tyler WJ, Hartman KN, Albeanu DF, Murthy VN (2005) Synaptic vesicle recycling studied in transgenic mice expressing synaptopHluorin. Proc Natl Acad Sci U S A 102:6131–6136.

Lima S, Milstien S, Spiegel S (2017) Sphingosine and sphingosine kinase 1 involvement in endocytic membrane trafficking. J Biol Chem 292:3074–3088.

Limanaqi F, Biagioni F, Gambardella S, Ryskalin L, Fornai F (2018) Interdependency between autophagy and synaptic vesicle trafficking: implications for dopamine release. Front Mol Neurosci 11:299.

Malik BR, Maddison DC, Smith GA, Peters OM (2019) Autophagic and endo-lysosomal dysfunction in neurodegenerative disease. Mol Brain 12:100.

Mao-Draayer Y, Sarazin J, Fox D, Schiopu E (2017) The sphingosine-1-phosphate receptor: a novel therapeutic target for multiple sclerosis and other autoimmune diseases. Clin Immunol 175:10–15.

McAdam RL, Morton A, Gordon SL, Alterman JF, Khvorova A, Cousin MA, Smillie KJ (2020) Loss of huntingtin function slows synaptic vesicle endocytosis in striatal neurons from the htt(Q140/Q140) mouse model of Huntington's disease. Neurobiol Dis 134:104637.

Menzies FM, et al. (2017) Autophagy and neurodegeneration: pathogenic mechanisms and therapeutic opportunities. Neuron 93:1015–1034.

Mizugishi K, Yamashita T, Olivera A, Miller GF, Spiegel S, Proia RL (2005) Essential role for sphingosine kinases in neural and vascular development. Mol Cell Biol 25:11113–11121.

Moruno Manchon JF, Uzor NE, Dabaghian Y, Furr-Stimming EE, Finkbeiner S, Tsvetkov AS (2015) Cytoplasmic sphingosine-1-phosphate pathway modulates neuronal autophagy. Sci Rep 5:15213.

Moruno Manchon JF, Uzor NE, Finkbeiner S, Tsvetkov AS (2016) SPHK1/sphingosine kinase 1-mediated autophagy differs between neurons and SH-SY5Y neuroblastoma cells. Autophagy 12:1418–1424.

Murthy VN, Stevens CF (1999) Reversal of synaptic vesicle docking at central synapses. Nat Neurosci 2:503–507.

Nawalpuri B, Sharma A, Chattarji S, Muddashetty RS (2021) Distinct temporal expression of the GW182 paralog TNRC6A in neurons regulates dendritic arborization. J Cell Sci 134:jcs258465.

Naylor J, Minard A, Gaunt HJ, Amer MS, Wilson LA, Migliore M, Cheung SY, Rubaiy HN, Blythe NM, Musialowski KE, Ludlow MJ, Evans WD, Green BL, Yang H, You Y, Li J, Fishwick CW, Muraki K, Beech DJ, Bon RS (2016) Natural and synthetic flavonoid modulation of TRPC5 channels. Br J Pharmacol 173:562–574.

Nichols RA, Dengler AF, Nakagawa EM, Bashkin M, Paul BT, Wu J, Khan GM (2007) A constitutive, transient receptor potential-like Ca2+ influx pathway in presynaptic nerve endings independent of voltage-gated Ca2+ channels and Na+/Ca2+ exchange. J Biol Chem 282:36102–36111.

Nofer JR, Bot M, Brodde M, Taylor PJ, Salm P, Brinkmann V, van Berkel T, Assmann G, Biessen EA (2007) FTY720, a synthetic sphingosine 1 phosphate analogue, inhibits development of atherosclerosis in low-density lipoprotein receptor-deficient mice. Circulation 115:501–508.

Overhoff M, De Bruyckere E, Kononenko NL (2021) Mechanisms of neuronal survival safeguarded by endocytosis and autophagy. J Neurochem 157:263–296.

Pan CY, Lee H, Chen CL (2006) Lysophospholipids elevate [Ca2+]i and trigger exocytosis in bovine chromaffin cells. Neuropharmacology 51:18–26.

Pensalfini A, Kim S, Subbanna S, Bleiwas C, Goulbourne CN, Stavrides PH, Jiang Y, Lee JH, Darji S, Pawlik M, Huo C, Peddy J, Berg MJ, Smiley JF, Basavarajappa BS, Nixon RA (2020) Endosomal dysfunction induced by directly overactivating Rab5 recapitulates prodromal and neurodegenerative features of Alzheimer's disease. Cell Rep 33:108420.

Pirhaji L, Milani P, Leidl M, Curran T, Avila-Pacheco J, Clish CB, White FM, Saghatelian A, Fraenkel E (2016) Revealing disease-associated pathways by network integration of untargeted metabolomics. Nat Methods 13:770–776.

Pitson SM, Moretti PA, Zebol JR, Xia P, Gamble JR, Vadas MA, D'Andrea RJ, Wattenberg BW (2000) Expression of a catalytically inactive sphingosine kinase mutant blocks agonist-induced sphingosine kinase activation. A dominant-negative sphingosine kinase. J Biol Chem 275:33945–33950.

Pitson SM, Moretti PA, Zebol JR, Zareie R, Derian CK, Darrow AL, Qi J, D'Andrea RJ, Bagley CJ, Vadas MA, Wattenberg BW (2002) The nucleotide-binding site of human sphingosine kinase 1. J Biol Chem 277:49545–49553.

Puram SV, Riccio A, Koirala S, Ikeuchi Y, Kim AH, Corfas G, Bonni A (2011) A TRPC5-regulated calcium signaling pathway controls dendrite patterning in the mammalian brain. Genes Dev 25:2659–2673.

Pyle JL, Kavalali ET, Piedras-Rentería ES, Tsien RW (2000) Rapid reuse of readily releasable pool vesicles at hippocampal synapses. Neuron 28:221–231.

Pyne NJ, Pyne S (2011) Selectivity and specificity of sphingosine 1-phosphate receptor ligands: "off-targets" or complex pharmacology? Front Pharmacol 2:26.

Pyszko JA, Strosznajder JB (2014) The key role of sphingosine kinases in the molecular mechanism of neuronal cell survival and death in an experimental model of Parkinson's disease. Folia Neuropathol 52:260–269.

Qi Y, Wang W, Chen J, Dai L, Kaczorowski D, Gao X, Xia P (2015) Sphingosine kinase 1 protects hepatocytes from lipotoxicity via down-regulation of IRE1α protein expression. J Biol Chem 290:23282–23290.

Ramsey IS, Delling M, Clapham DE (2006) An introduction to TRP channels. Annu Rev Physiol 68:619–647.

Regehr WG (2012) Short-term presynaptic plasticity. Cold Spring Harb Perspect Biol 4:a005702.

Rennick JJ, Johnston APR, Parton RG (2021) Key principles and methods for studying the endocytosis of biological and nanoparticle therapeutics. Nat Nanotechnol 16:266–276.

Ribeiro LF, Verpoort B, Nys J, Vennekens KM, Wierda KD, de Wit J (2019) SorCS1-mediated sorting in dendrites maintains neurexin axonal surface polarization required for synaptic function. PLoS Biol 17:e3000466.

Riganti L, Antonucci F, Gabrielli M, Prada I, Giussani P, Viani P, Valtorta F, Menna E, Matteoli M, Verderio C (2016) Sphingosine-1-phosphate (S1P) impacts presynaptic functions by regulating synapsin I localization in the presynaptic compartment. J Neurosci 36:4624–4634.

Rizzoli SO (2014) Synaptic vesicle recycling: steps and principles. EMBO J 33:788–822.

Royle SJ, Granseth B, Odermatt B, Derevier A, Lagnado L (2008) Imaging phluorin-based probes at hippocampal synapses. Methods Mol Biol 457:293–303.

Ryan TA, Smith SJ (1995) Vesicle pool mobilization during action potential firing at hippocampal synapses. Neuron 14:983–989.

Sadler KE, Moehring F, Shiers SI, Laskowski LJ, Mikesell AR, Plautz ZR, Brezinski AN, Mecca CM, Dussor G, Price TJ, McCorvy JD, Stucky CL (2021) Transient receptor potential canonical 5 mediates inflammatory mechanical and spontaneous pain in mice. Sci Transl Med 13:eabd7702.

Saheki Y, De Camilli P (2012) Synaptic vesicle endocytosis. Cold Spring Harb Perspect Biol 4:a005645.

Sanna MG, Wang SK, Gonzalez-Cabrera PJ, Don A, Marsolais D, Matheu MP, Wei SH, Parker I, Jo E, Cheng WC, Cahalan MD, Wong CH, Rosen H (2006) Enhancement of capillary leakage and restoration of lymphocyte egress by a chiral S1P1 antagonist in vivo. Nat Chem Biol 2:434–441.

Sawamura S, Shirakawa H, Nakagawa T, Mori Y, Kaneko S (2017) TRP channels in the brain: what are they there for? In: Neurobiology of TRP channels (EmirTLR, ed), pp 295–322. Boca Raton: CRC Press/Taylor & Francis.

Schikorski T, Stevens CF (2001) Morphological correlates of functionally defined synaptic vesicle populations. Nat Neurosci 4:391–395.

Schreij AM, Fon EA, McPherson PS (2016) Endocytic membrane trafficking and neurodegenerative disease. Cell Mol Life Sci 73:1529–1545.

Schwarz Y, Oleinikov K, Schindeldecker B, Wyatt A, Weißgerber P, Flockerzi V, Boehm U, Freichel M, Bruns D (2019) TRPC channels regulate Ca2+-signaling and short-term plasticity of fast glutamatergic synapses. PLoS Biol 17:e3000445.

Shen H, Giordano F, Wu Y, Chan J, Zhu C, Milosevic I, Wu X, Yao K, Chen B, Baumgart T, Sieburth D, De Camilli P (2014) Coupling between endocytosis and sphingosine kinase 1 recruitment. Nat Cell Biol 16:652–662.

Silva VR, Micheletti TO, Pimentel GD, Katashima CK, Lenhare L, Morari J, Mendes MC, Razolli DS, Rocha GZ, de Souza CT, Ryu D, Prada PO, Velloso LA, Carvalheira JB, Pauli JR, Cintra DE, Ropelle ER (2014) Hypothalamic S1P/S1PR1 axis controls energy homeostasis. Nat Commun 5:4859.

Sim-Selley LJ, Goforth PB, Mba MU, Macdonald TL, Lynch KR, Milstien S, Spiegel S, Satin LS, Welch SP, Selley DE (2009) Sphingosine-1-phosphate receptors mediate neuromodulatory functions in the CNS. J Neurochem 110:1191–1202.

Soykan T, Maritzen T, Haucke V (2016) Modes and mechanisms of synaptic vesicle recycling. Curr Opin Neurobiol 39:17–23.

Soykan T, Kaempf N, Sakaba T, Vollweiter D, Goerdeler F, Puchkov D, Kononenko NL, Haucke V (2017) Synaptic vesicle endocytosis occurs on multiple timescales and is mediated by formin-dependent actin assembly. Neuron 93:854–866.e4.

Spiegel S, Milstien S (2003) Sphingosine-1-phosphate: an enigmatic signalling lipid. Nat Rev Mol Cell Biol 4:397–407.

Stessin AM, Gursel DB, Schwartz A, Parashar B, Kulidzhanov FG, Sabbas AM, Boockvar J, Nori D, Wernicke AG (2012) FTY720, sphingosine 1-phosphate receptor modulator, selectively radioprotects hippocampal neural stem cells. Neurosci Lett 516:253–258.

Strübing C, Krapivinsky G, Krapivinsky L, Clapham DE (2003) Formation of novel TRPC channels by complex subunit interactions in embryonic brain. J Biol Chem 278:39014–39019.

Subei AM, Cohen JA (2015) Sphingosine 1-phosphate receptor modulators in multiple sclerosis. CNS Drugs 29:565–575.

Trkov S, Stenovec M, Kreft M, Potokar M, Parpura V, Davletov B, Zorec R (2012) Fingolimod–a sphingosine-like molecule inhibits vesicle mobility and secretion in astrocytes. Glia 60:1406–1416.

Varga K, Jiang ZJ, Gong LW (2020) Phosphatidylserine is critical for vesicle fission during clathrin-mediated endocytosis. J Neurochem 152:48–60.

Venkatachalam K, Montell C (2007) TRP channels. Annu Rev Biochem 76:387–417.

Vevea JD, Chapman ER (2020) Acute disruption of the synaptic vesicle membrane protein synaptotagmin 1 using knockoff in mouse hippocampal neurons. Elife 9:e56469.

Voglmaier SM, Kam K, Yang H, Fortin DL, Hua Z, Nicoll RA, Edwards RH (2006) Distinct endocytic pathways control the rate and extent of synaptic vesicle protein recycling. Neuron 51:71–84.

Wang Y, Balaji V, Kaniyappan S, Krüger L, Irsen S, Tepper K, Chandupatla R, Maetzler W, Schneider A, Mandelkow E, Mandelkow EM (2017) The release and trans-synaptic transmission of Tau via exosomes. Mol Neurodegener 12:5.

Weth-Malsch D, Langeslag M, Beroukas D, Zangrandi L, Kastenberger I, Quarta S, Malsch P, Kalpachidou T, Schwarzer C, Proia RL, Haberberger RV, Kress M (2016) Ablation of sphingosine 1-phosphate receptor

subtype 3 impairs hippocampal neuron excitability in vitro and spatial working memory in vivo. Front Cell Neurosci 10:258.
Willems LM, Zahn N, Ferreirós N, Scholich K, Maggio N, Deller T, Vlachos A (2016) Sphingosine-1-phosphate receptor inhibition prevents denervation-induced dendritic atrophy. Acta Neuropathol Commun 4:28.
Wu XS, Wu LG (2014) The yin and yang of calcium effects on synaptic vesicle endocytosis. J Neurosci 34:2652–2659.
Wu XS, McNeil BD, Xu J, Fan J, Xue L, Melicoff E, Adachi R, Bai L, Wu LG (2009) Ca(2+) and calmodulin initiate all forms of endocytosis during depolarization at a nerve terminal. Nat Neurosci 12:1003–1010.
Xu H, Delling M, Jun JC, Clapham DE (2006) Oregano, thyme and clove-derived flavors and skin sensitizers activate specific TRP channels. Nat Neurosci 9:628–635.
Yang S, Park D, Manning L, Hill SE, Cao M, Xuan Z, Gonzalez I, Dong Y, Clark B, Shao L, Okeke I, Almoril-Porras A, Bai J, De Camilli P, Colón-Ramos DA (2022) Presynaptic autophagy is coupled to the synaptic vesicle cycle via ATG-9. Neuron 110:824–840.e10.
Yao CK, Lin YQ, Ly CV, Ohyama T, Haueter CM, Moiseenkova-Bell VY, Wensel TG, Bellen HJ (2009) A synaptic vesicle-associated Ca2+ channel promotes endocytosis and couples exocytosis to endocytosis. Cell 138:947–960.
Yao CK, Liu YT, Lee IC, Wang YT, Wu PY (2017) A Ca2+ channel differentially regulates Clathrin-mediated and activity-dependent bulk endocytosis. PLoS Biol 15:e2000931.
Yao LH, Rao Y, Varga K, Wang CY, Xiao P, Lindau M, Gong LW (2012) Synaptotagmin 1 is necessary for the Ca2+ dependence of clathrin-mediated endocytosis. J Neurosci 32:3778–3785.
Yao LH, Rao Y, Bang C, Kurilova S, Varga K, Wang CY, Weller BD, Cho W, Cheng J, Gong LW (2013) Actin polymerization does not provide direct mechanical forces for vesicle fission during clathrin-mediated endocytosis. J Neurosci 33:15793–15798.
Yin P, Xue Y, Wang T, Zhong D, Li G (2021) The therapeutic targets of fingolimod (FTY720) are involved in pathological processes in the frontal cortex of Alzheimer's disease patients: a network pharmacology study. Front Aging Neurosci 13:609679.
Yonamine I, Bamba T, Nirala NK, Jesmin N, Kosakowska-Cholody T, Nagashima K, Fukusaki E, Acharya JK, Acharya U (2011) Sphingosine kinases and their metabolites modulate endolysosomal trafficking in photoreceptors. J Cell Biol 192:557–567.
Young MM, Takahashi Y, Fox TE, Yun JK, Kester M, Wang HG (2016) Sphingosine kinase 1 cooperates with autophagy to maintain endocytic membrane trafficking. Cell Rep 17:1532–1545.
Zhang Y, Li X, Ciric B, Ma CG, Gran B, Rostami A, Zhang GX (2017) Effect of fingolimod on neural stem cells: a novel mechanism and broadened application for neural repair. Mol Ther 25:401–415.
Zucker RS, Regehr WG (2002) Short-term synaptic plasticity. Annu Rev Physiol 64:355–405.